Monthly Notices
of the
ROYAL ASTRONOMICAL SOCIETY

MNRAS **437,** 1976–1995 (2014)
Advance Access publication 2013 November 15

doi:10.1093/mnras/stt2028

Quasar broad absorption line variability measurements using reconstructions of unabsorbed spectra

C. Wildy,[1]⋆ M. R. Goad[1] and J. T. Allen[2]

[1]*University of Leicester, Department of Physics and Astronomy, University Road, Leicester LE1 7RH, UK*
[2]*Sydney Institute for Astronomy, School of Physics, A28, The University of Sydney, NSW 2006, Australia*

Accepted 2013 October 18. Received 2013 October 8; in original form 2013 August 15

ABSTRACT

We present a two-epoch Sloan Digital Sky Survey and Gemini/GMOS+William Herschel Telescope/ISIS variability study of 50 broad absorption line (BAL) quasars of redshift range $1.9 < z < 4.2$, containing 38 Si IV and 59 C IV BALs and spanning rest-frame time intervals of ≈10 months to 3.7 years. We find that 35/50 quasars exhibit one or more variable BALs, with 58 per cent of Si IV and 46 per cent of C IV BALs showing variability across the entire sample. On average, Si IV BALs show larger fractional change in BAL pseudo-equivalent width than C IV BALs, as referenced to an unabsorbed continuum+emission line spectrum constructed using non-negative matrix factorization. No correlation is found between BAL variability and quasar luminosity, suggesting that ionizing continuum changes do not play a significant role in BAL variability (assuming the gas is in photoionization equilibrium with the ionizing continuum). A subset of 14 quasars have one variable BAL from each of Si IV and C IV with significant overlap in velocity space and for which variations are in the same sense (strengthening or weakening) and which appear to be correlated (98 per cent confidence). We find examples of both appearing and disappearing BALs in weaker/shallower lines with disappearance rates of 2.3 per cent for C IV and 5.3 per cent for Si IV, suggesting average lifetimes of 142 and 43 years, respectively. We identify five objects in which the BAL is coincident with the broad emission line, but appears to cover only the continuum source. Assuming a clumpy inhomogeneous absorber model and a typical size for the continuum source, we infer a maximum cloud radius of 10^{13} to 10^{14} cm, assuming Eddington limited accretion.

Key words: galaxies: active – quasars: absorption lines – quasars: general.

1 INTRODUCTION

Broad absorption line quasars (BALQSOs) show evidence of high-velocity outflows in the form of strong, blueshifted broad absorption lines (BALs). Previous quasar spectral studies have indicated that this subcategory comprises 10–20 per cent of the QSO population (Reichard et al. 2003a; Knigge et al. 2008; Scaringi et al. 2009), although the intrinsic fraction may be as high as 41 per cent if differential Sloan Digital Sky Survey (SDSS) target selection effects are taken into account (Allen et al. 2011).

The BALs, by definition, comprise absorption troughs in which the flux is less than 90 per cent of the continuum level, extending over at least 2000 km s^{-1} in the quasar rest frame (Weymann et al. 1991). They are one of three examples of blueshifted absorption features seen in AGN, others being narrow absorption lines (NALs), with velocity widths of a few hundred km s^{-1}, and mini-BALs, with velocity widths intermediate to those of NALs and BALs (Narayanan et al. 2004). The outflows giving rise to these absorption lines are thought to originate in accretion disc instabilities and are accelerated to velocities of up to 0.2c in the quasar rest frame (Hamann et al. 2013) by radiation pressure (Elvis 2000; Proga, Stone & Kallman 2000; Chelouche & Netzer 2001), magnetic effects (Blandford & McKee 1982; Everett 2005) or thermal winds (Bottorff et al. 1997; Giustini & Proga 2012) from the accretion disc. The fraction of quasars presenting BALs can be interpreted as an orientation effect, with this fraction being a measure of the proportion of the sky as seen from the quasar which is covered by the outflow. Large-scale outflows may therefore occur in a much greater fraction of the quasar population than the BAL fraction would imply (Schmidt & Hines 1999).

The flows have been theorised to extend as far as a few hundred parsecs from the central engine (Barlow 1994), allowing the kinetic energy to be transferred to the interstellar medium. This process may be responsible for quenching star formation in the host galaxy and limiting black hole growth (Springel, Di Matteo & Hernquist

⋆E-mail: cw268@le.ac.uk

2005; King 2010). It may also result in the observed relationship between the masses of supermassive black holes and galactic bulges (Magorrian et al. 1998; Silk & Rees 1998).

The most common (∼85 per cent) BALQSO subtype is the high-ionization BALQSOs (HiBALs) whose spectra only show broad absorption due to high-ionization transitions such as C IV λ1549, Si IV λ1400 and N V λ1240 (Sprayberry & Foltz 1992; Reichard et al. 2003b). The remaining proportion, known as low-ionization BALQSOs (LoBALs) show broad absorption resulting from low-ionization species such as Mg II, Al III and on rare occasions Fe II (known as FeLoBALs) in addition to Hi-BALs.

Several studies now exist which probe the spectral variability of BALs in BALQSOs over a range of object rest-frame time-scales from approximately one week to several years (Barlow 1994; Lundgren et al. 2007; Gibson et al. 2008, 2010; Capellupo et al. 2011, 2012, 2013). Measurements of quasar variability can provide valuable insights into the properties of the central engine. It is known that photoionization effects resulting from changes in the ionizing continuum drive the observed broad emission line (BEL) variability (Peterson et al. 1998; Vanden Berk, Wilhite & Kron 2004; Wilhite et al. 2006); however, the mechanism responsible for BAL variations is less secure. Variability studies of BALs can prove important in identifying the geometry of the outflows as well as constraining the range of physical conditions that result in variability, especially since previous results have proved contradictory or inconclusive. Evidence has been put forward in favour of ionization state changes (Barlow 1994), movement of gas along the line of sight to the quasar emission region (Gibson et al. 2008; Hamann et al. 2008) or a combination of both effects (Capellupo et al. 2012).

Many previous studies have focused on C IV BAL variability only (Lundgren et al. 2007; Gibson et al. 2008; Capellupo et al. 2011; Filiz Ak et al. 2012), however recent efforts have also included significant Si IV investigations (Gibson et al. 2010; Capellupo et al. 2012). We examine variability in both ions from a sample consisting mostly of HiBAL QSOs. Of the previous investigations into C IV BALs, Lundgren et al. (2007, hereafter referred to as L07) and Filiz Ak et al. (2012) used minimum velocity cutoffs to avoid the difficulties associated with properly identifying and quantifying absorption where BELs overlap with the corresponding absorption line. Many BALQSOs show evidence of absorption of both continuum and emission flux by the BAL outflow (Turnshek 1988), meaning that in cases of BAL/BEL overlap, more light is removed from the line of sight than a continuum-based BAL depth measurement would suggest. We address these issues by attempting to quantify variability in BALs which include features down to zero velocity using reconstructions of the unabsorbed quasar spectrum over the wavelength range of interest. As well as solving the problem of introducing a low velocity cutoff, this allows measurements to be taken for cases of high velocity ($>13\,500\,\mathrm{km\,s^{-1}}$) Si IV outflows, which may overlap with the O I λ1304 and C II λ1334 emission lines (Trump et al. 2006). Using the method of Allen et al. (2011), we produce reconstructions of the underlying continuum plus emission spectra for each of the quasars in our sample using non-negative matrix factorization (NMF), a blind source separation technique. We use this unabsorbed spectrum as a pseudo-continuum from which BAL pseudo-equivalent width (EW) measurements are made.

The ionization energies of Si III and Si IV are 33.5 and 45.1 eV, respectively, while the ionization energies of C III and C IV are 47.9 and 64.5 eV, respectively. The abundances of carbon and silicon are also assumed to be unequal (Hamann et al. 2011). Differing variability properties of Si IV and C IV can therefore inform attempts to explain the physics, kinematics and geometry of outflows which result in BAL variability. A significant fraction (41 out of 50 quasars) of our sample contain both Si IV and C IV BALs, allowing direct comparison in the behaviour of the two ions in these quasars.

Throughout this paper, all time intervals are measured in days in the quasar rest frame. We assume a flat Λ cold dark matter cosmology with $H_0 = 70\,\mathrm{km\,s^{-1}\,Mpc^{-1}}$, $\Omega_M = 0.3$ and $\Omega_\Lambda = 0.7$.

2 SAMPLE SELECTION AND OBSERVATIONS

2.1 The Balnicity index

A common method used to identify a quasar as a BALQSO is to consider a quantity known as the Balnicity index (BI), originally defined by Weymann et al. (1991) for C IV BALs. The BI is a modified EW measurement which is zero for non-BALQSOs and positive for BALQSOs. The BI is defined as

$$\mathrm{BI} = \int_{-25\,000}^{-3000} \left[1 - \frac{f(v)}{0.9}\right] C\,\mathrm{d}v, \tag{1}$$

where $f(v)$ is the continuum-normalized flux as a function of outflow velocity v relative to line centre and C is a constant equal to unity when $f(v)$ has been under 90 per cent of the continuum level over the previous $2000\,\mathrm{km\,s^{-1}}$ of the integration range and zero otherwise. The upper velocity boundary avoids confusion between C IV outflows and the Si IV emission line. The lower velocity boundary avoids absorption line overlap with the transition's BEL. An alternative to the BI is the absorption index (AI) defined in Hall et al. (2002). The AI modifies the BI so that it requires at least a contiguous $450\,\mathrm{km\,s^{-1}}$ of absorption at below the 90 per cent continuum level to register a positive value rather than $2000\,\mathrm{km\,s^{-1}}$ and reduces the lower velocity limit to $0\,\mathrm{km\,s^{-1}}$.

2.2 Sample selection

A redshift range of approximately $1.9 < z < 4.1$ was selected so that the spectral region from the continuum band at 1350 Å to the continuum redward of C IV λ1549 was observable. Variability is tested across two epochs, hereafter referred to as epoch 1 and epoch 2 for the earlier and later observations, respectively, covering a rest-frame time-scale of ≈10 months to 3.7 years. This epoch separation time-scale is relatively unexplored in previous BAL variability studies. Epoch 1 uses spectral data from objects imaged as part of the SDSS, while epoch 2 observations were obtained from either the William Herschel Telescope (WHT) or the Gemini Observatories.

The BALQSOs observed as part of this study were selected from the BALQSO catalogue of Scaringi et al. (2009). This catalogue comprises 3552 BALQSOs and was compiled from a parent sample of 28 421 QSOs published in the 5th data release (DR5) of the SDSS (Adelman-McCarthy et al. 2007) using a hybrid classification scheme comprising a combination of simple metrics (e.g. BI), a supervised neural network and visual inspection.

From the parent sample of 3552 BALQSOs, we select only those objects tagged as definitely real (1353), and with $\mathrm{BI} > 2000\,\mathrm{km\,s^{-1}}$ to minimize contamination by (possibly unrelated) NAL systems. A total of 595 objects satisfy all of these criteria. From this sample, objects were selected to span a broad range in balnicity ($\mathrm{BI} > 2000\,\mathrm{km\,s^{-1}}$), redshift ($z > 2$) and luminosity ($-28.75 < M_i < -25.75$). Of the 50 objects from this sample observed as part of this programme, a Kolmogorov–Smirnov (K-S) test, on the distribution functions of their observed properties (BI, z, M_i), shows that they are statistically consistent with those of the parent BALQSO population.

Non-BALQSO continuum variability is known to scale inversely with object luminosity and directly with redshift (Vanden Berk et al. 2004). As BALQSOs seem to be part of the same parent population as non-BALQSOs (Reichard et al. 2003b) and given that ionization is the main driver of variability in non-BALQSOs (Blandford & McKee 1982; Peterson et al. 1998), if ionizing continuum variations produce the variability seen in BALs it may be expected that lower luminosity BALQSOs would show the greatest BAL variations. In order to test the relationship between luminosity and variability our BALQSO sample spans a factor of 10 in *i*-band source luminosity. The redshift distribution of the BALQSOs from our original sample observed as part of this campaign peaks at the lower limit of our sample redshift range and is too small to give statistically reliable measurements of the dependence of BAL variability on redshift.

2.3 The Sloan Digital Sky Survey

Epoch 1 observations were obtained from DR6 of the SDSS. Beginning in 2000, the SDSS had imaged approximately 10 000 deg^2 of the sky as of 2000 June (Schneider et al. 2010), using the 2.5 m telescope at the Apache Point Observatory, New Mexico, USA (York 2000). Imaging is carried out using a CCD camera that operates in drift-scanning mode (Gunn et al. 1998). Five broad-band filters, *u*, *g*, *r*, *i* and *z*, normalized to the AB system, are used, covering a wavelength range of 3900 to 9100 Å with an approximate spectral resolution of $\lambda/\Delta\lambda = 2000$ at 5000 Å (Stoughton et al. 2002). Further information on the SDSS data reduction process is given in Lupton et al. (2001) and Stoughton et al. (2002).

2.4 Gemini-North and -South observatories

The Gemini Multi-Object Spectrograph (GMOS) instruments, located on the Gemini-North and Gemini-South telescopes are spectrographs consisting of three CCD detectors separated by gaps corresponding to 39 unbinned pixels, which were used to obtain data for 44 target observations in long-slit mode. Five of these observations were excluded from the final sample due to cloud cover issues, insufficient integration time or a deficiency of spectral regions containing unabsorbed continuum.

A slit width of 1.5 arcsec was used at both locations for all Gemini observations. The grating configurations employed blaze wavelengths such that the spectral region of interest, extending from 1350 Å to C IV λ1549 in the quasar rest frame, was included in the total wavelength span. The B600 grating (resolution $\Delta\lambda/\lambda \approx 1688$ at blaze wavelength 4610 Å) and R400 grating (resolution $\Delta\lambda/\lambda \approx 1918$ at blaze wavelength 7640 Å) were used. Three were observed in semester A 2008, the rest throughout 2011 and early 2012. Details of Gemini/GMOS observations are given in Table 1 (lower panel).

The GMOS spectra were reduced using version 1.11 of the Gemini IRAF package, initially applying bias correction using zero time exposures and using flat-field images to correct for illumination differences and pixel-to-pixel sensitivity variations in the CCD images. Spectra were extracted using the IRAF optimal extraction routine using a width of 10 pixels. Wavelength calibration and flux calibration were applied using arc line exposures and observations of photometric standard stars, respectively. Arc exposures and standard star observations were obtained during the observing nights. Sky background subtraction was also applied to the extracted spectra to remove much of the atmospheric background contaminating the data. Details of each Gemini object observation are given in Table 1 (lower panel).

2.5 The William Herschel Telescope

The WHT Intermediate dispersion Spectrograph and Imaging System (ISIS) spectrograph was used for long-slit spectroscopy of eight targets during semester A 2008, taken as part of a previous investigation into radiative line driving (Cottis et al. 2010). Observations were taken with the ISIS double-armed (red and blue arm) spectrograph using the 5700 dichroic allowing simultaneous observations at both short and long wavelengths. For each object, spectra from the two arms in the overlapping range 5400 to 5700 Å were combined using an error weighted mean in each wavelength bin. Observations were performed in long-slit mode with the R158B and R158R gratings, giving a nominal spectral resolution of 1.6 Å per pixel in the blue and 1.8 Å per pixel in the red. A slit width of 1.5 arcsec was chosen to match typical seeing conditions and give reasonable throughput without compromising the spectral resolution. For each source, multiple exposures were taken (in order to remove cosmic ray hits) bracketed by arc-lamp exposures for wavelength calibration. Standard star spectra were taken on the observing nights to allow flux calibration of the targets. As in the Gemini/GMOS observations, correction of CCD images using bias and flat-field exposures was performed, this time within the IRAF *ccdproc* routine. Spectra were extracted, along with sky background removal, using the *apall* task within the IRAF *longslit* package. Wavelength and flux calibration were applied to the extracted spectra within this same package.

Details of each WHT object observation are given in Table 1 (upper panel).

3 RECONSTRUCTION METHOD

The unabsorbed continuum plus emission line spectra – the pseudo-continuum spectra – were reconstructed using the NMF method described in Allen et al. (2011). For the epoch 1 (SDSS) spectra, the reconstructions were the same as those used in Allen et al. (2011); new fits were produced for the epoch 2 (Gemini and WHT) spectra, with some minor modifications to the method. Full details are provided in Allen et al. (2011); here we provide a summary of the method and the necessary modifications.

Before any analyses were performed on the data, all SDSS, Gemini and WHT spectra were corrected for the effects of Milky Way Galactic Extinction using the method of Cardelli, Clayton & Mathis (1989) with A_V values taken from Schlegel, Finkbeiner & Davis (1998). All following processing steps were all performed in the quasar rest frame, using the redshifts derived by Hewett & Wild (2010).

Input samples of up to 500 spectra in each $\Delta z = 0.1$ redshift bin were drawn from the sample of SDSS DR6 quasar spectra *without* broad absorption. Each of these input samples was processed using NMF to produce a set of 8–14 component spectra. These components can be linearly combined to reconstruct the spectrum of each of the input quasars. The number of components was selected independently for each redshift bin, and was set to be the greatest number that could be generated before overfitting occurred. Overfitted spectra are identified as those having much lower χ^2_ν values than others in the input sample.

Once the component spectra had been generated, they could then be fitted to each BALQSO spectrum. Because the component spectra were based on non-BAL quasar spectra, the resulting reconstructions are of the unabsorbed pseudo-continuum. To perform this fit, the Gemini and WHT spectra were placed on the SDSS logarithmic wavelength scale, using a linear interpolation between pixels. An

Table 1. WHT/ISIS (upper panel) and Gemini/GMOS (lower panel) long-slit spectroscopic observations of SDSS quasars.

Object	z	Absolute i-band magnitude M_i	Exp. time (s)	Grating	Mean airmass
SDSSJ101844.45+544015.6[d]	3.251 ± 0.004	−26.852	3 × 1500	R158B and R158R	1.26
SDSSJ113831.42+351725.3[d]	2.122 ± 0.002	−26.891	3 × 1200	R158B and R158R	1.14
SDSSJ114704.47+153243.3[d]	3.092 ± 0.002	−27.848	2 × 1200	R158B and R158R	1.29
SDSSJ134458.82+483457.5[d]	2.048 ± 0.002	−26.709	3 × 1500	R158B and R158R	1.24
SDSSJ162657.47+405848.0[d]	3.062 ± 0.003	−27.576	4 × 1400	R158B and R158R	1.04
SDSSJ164152.30+305851.7[d]	2.016 ± 0.002	−27.831	3 × 1500	R158B and R158R	1.06
SDSSJ170056.85+602639.7[d]	2.136 ± 0.002	−27.367	3 × 1400	R158B and R158R	1.25
SDSSJ212412.60+095923.3[d]	1.921 ± 0.002	−26.665	3 × 1200	R158B and R158R	1.17
SDSSJ001025.90+005447.6	2.861 ± 0.002	−27.806	2 × 600	B600+G5323	1.54
SDSSJ004613.54+010425.7	2.149 ± 0.002	−28.404	2 × 600	B600+G5323	1.32
SDSSJ025720.43−080322.5	2.045 ± 0.005	−26.786	2 × 1500	B600+G5323	1.37
SDSSJ031033.45−060957.8	2.050 ± 0.002	−27.424	2 × 900	B600+G5323	1.26
SDSSJ031331.22−070422.8	2.777 ± 0.002	−27.844	2 × 1200	B600+G5323	1.51
SDSSJ032832.77−070750.3[a]	2.917 ± 0.005	−27.223	2 × 1500	B600+G5323	1.36
SDSSJ033223.51−065450.5	3.708 ± 0.008	−27.646	1 × 1500	B600+G5323	1.10
SDSSJ033224.95−062116.1	2.761 ± 0.002	−27.487	2 × 900	B600+G5323	1.50
SDSSJ034946.61−065730.3[b]	3.973 ± 0.011	−27.313	2 × 1800	B600+G5323	1.27
SDSSJ035335.67−061802.5	2.165 ± 0.002	−27.218	2 × 1200	B600+G5323	1.67
SDSSJ035749.11−061121.9	2.006 ± 0.002	−26.976	2 × 1400	B600+G5323	1.53
SDSSJ073535.44+374450.4	2.751 ± 0.002	−28.259	1 × 1500	B600+G5307	1.10
SDSSJ081823.46+484910.8	2.015 ± 0.002	−26.584	4 × 900	B600+G5307	1.28
SDSSJ081925.00+032455.7	2.239 ± 0.002	−27.022	2 × 600	B600+G5323	1.36
SDSSJ082813.47+065326.4	2.968 ± 0.004	−27.779	2 × 900	B600+G5323	1.35
SDSSJ083718.63+482806.1	3.646 ± 0.003	−28.484	1 × 1200	B600+G5307	1.25
SDSSJ084023.51+063739.1[c]	3.801 ± 0.010	−27.170	1 × 1362	B600+G5323	1.25
SDSSJ084408.29+423226.9	2.964 ± 0.002	−28.215	1 × 1500	B600+G5307	1.40
SDSSJ085006.08+072959.0	2.690 ± 0.002	−28.622	2 × 300	B600+G5323	1.41
SDSSJ085104.05+051539.8[d]	3.222 ± 0.003	−28.480	6 × 600	B600+G5303	1.04
SDSSJ092557.52+044035.9	2.271 ± 0.002	−27.174	2 × 600	B600+G5323	1.53
SDSSJ092639.34+383656.7	2.155 ± 0.002	−27.292	2 × 1200	B600+G5307	1.32
SDSSJ093251.98+023727.0	2.169 ± 0.002	−28.106	2 × 400	B600+G5323	1.37
SDSSJ095224.84+064732.0	2.174 ± 0.002	−27.877	2 × 400	B600+G5323	1.42
SDSSJ100021.72+035116.5	2.017 ± 0.002	−27.314	1 × 600	B600+G5323	1.32
SDSSJ100312.63+402505.6	3.247 ± 0.003	−27.342	3 × 900	B600+G5307	1.38
SDSSJ101056.68+355833.3	2.301 ± 0.002	−27.334	1 × 1200	B600+G5307	1.04
SDSSJ104059.79+055524.4	2.450 ± 0.002	−27.023	2 × 1500	B600+G5323	1.40
SDSSJ105334.57+425724.9	2.719 ± 0.003	−27.221	4 × 900	B600+G5307	1.17
SDSSJ110041.19+003631.9	2.020 ± 0.002	−27.497	2 × 600	B600+G5323	1.22
SDSSJ110339.90+011928.5	2.056 ± 0.002	−27.203	2 × 600	B600+G5323	1.28
SDSSJ111516.08+460234.6[c]	4.175 ± 0.010	−27.376	1 × 721 and 1 × 900	R400+G5305	1.16
SDSSJ112733.69+343008.8	4.060 ± 0.009	−28.594	4 × 900	R400+G5305	1.06
SDSSJ114722.09+373720.7	2.199 ± 0.002	−26.380	4 × 900	B600+G5307	1.05
SDSSJ115007.66+542737.1[d]	3.534 ± 0.004	−28.016	6 × 600	R400+G5305	1.22
SDSSJ125628.67+393548.0	2.138 ± 0.002	−27.309	1 × 1200	B600+G5307	1.07
SDSSJ142244.45+382330.6[d]	3.741 ± 0.010	−28.566	6 × 600	R400+G5305	1.06
SDSSJ143604.64+350428.5	3.035 ± 0.006	−26.625	3 × 900	B600+G5307	1.04
SDSSJ143632.25+501403.6	2.784 ± 0.002	−27.502	2 × 1500	B600+G5307	1.67
SDSSJ151601.51+430931.4	2.610 ± 0.002	−28.373	2 × 1200	B600+G5307	1.11
SDSSJ153226.22+313138.1[c]	2.889 ± 0.003	−28.194	1 × 336 and 1 × 1200	B600+G5307	1.21
SDSSJ165248.29+325032.3	2.832 ± 0.008	−26.558	1 × 1500	B600+G5307	1.03
SDSSJ205659.48−071123.1	2.083 ± 0.002	−27.547	2 × 900	B600+G5323	1.10
SDSSJ210436.62−070738.3	2.360 ± 0.004	−27.268	2 × 1500	B600+G5323	1.17
SDSSJ211718.17+010248.9	2.928 ± 0.003	−27.550	2 × 1500	B600+G5323	1.17
SDSSJ213138.93−070013.3	2.045 ± 0.002	−27.425	2 × 900	B600+G5323	1.37
SDSSJ222505.28−084542.7	2.085 ± 0.003	−27.121	2 × 900	B600+G5323	1.17

[a]Excluded due to lack of observable continuum bands <1549 Å.
[b]Excluded due to 80 per cent cloud cover.
[c]Excluded due to shortened integration time.
[d]Observed in 2008.
Redshifts taken from Hewett & Wild (2010).

iterative procedure was used to mask out the absorption regions from the fit. At each step in this procedure, the component spectra were fit to the observed spectrum using the current mask, and a new mask was generated by searching for regions where the observed flux fell significantly below the reconstruction. The iteration continued until the change in the mask from one step to the next was small.

For the SDSS spectra, the most highly reddened quasars were given an empirical dust correction, assuming a power-law reddening curve, to match their overall shape to that of a typical quasar at the same redshift. After the component spectra were fitted to the de-reddened spectrum, both the BALQSO spectrum and the reconstruction had the dust correction removed, matching the reconstruction to the shape of the original observed spectrum. For the Gemini and WHT spectra, the spectral coverage was insufficient to give reliable measurements of the continuum slope. However, the three objects in the original sample whose SDSS continua required a reddening correction (J032832.77−070750.3, J034946.61−065730.3 and J111516.08+460234.6) were all excluded for other reasons; we hence assumed that no such corrections were required for the Gemini and WHT spectra of the remaining objects.

For the SDSS spectra, unphysical reconstructed emission line profiles in C IV were detected automatically and corrected by reducing the number of components used in the fit. Additionally, spectra that failed certain automated quality control measurements were visually inspected for failures in the automatic masking procedure, and in such cases a manually defined mask was applied and the components re-fitted. For the Gemini and WHT data, the small number of spectra meant that they could all be visually inspected for both of these potential problems. The same corrections as for SDSS spectra were applied in the cases where unphysical emission line profiles or poorly defined masks were seen. Of the 35 quasars with variable BALs, three required corrections because of their emission line profiles and nine because of poor automatic masks. The higher rate of manual intervention relative to SDSS spectra is primarily due to the smaller wavelength range of the Gemini spectra, and does not affect the quality of the final reconstructions.

The uncertainty on the reconstructed flux level was determined using the synthetic BALQSO spectra described in section 7.1 of Allen et al. (2011). A sample of 50 non-BAL quasars was selected in each redshift bin, and a series of BAL troughs with known depth and shape was inserted into each spectrum. Extra noise was also added. The modified spectra were run through the same pseudo-continuum fitting procedure as the observed spectra. The fits derived in this way were then compared to the fits produced for the original unabsorbed spectra in the wavelength range of the inserted BAL trough, defined as all pixels with a (known) flux ratio <0.9. We characterized the error in each spectrum using the root mean square (rms) of the fractional difference between reconstructions, then took the median value of this rms over all spectra in each bin of redshift and signal-to-noise ratio (S/N). The resulting uncertainty was assumed to be dominated by the uncertainty in the normalization of the pseudo-continuum, rather than its shape, resulting in the errors in all pixels being perfectly correlated with each other.

The above steps produced a reconstruction of the unabsorbed pseudo-continuum for each observed spectrum. For a given BALQSO, the reconstructions of the two epochs were derived in a consistent fashion, having used the same NMF components and the same fitting algorithms, but are independent of each other. Example reconstructions for the two observations of a single BALQSO are shown in Fig. 1.

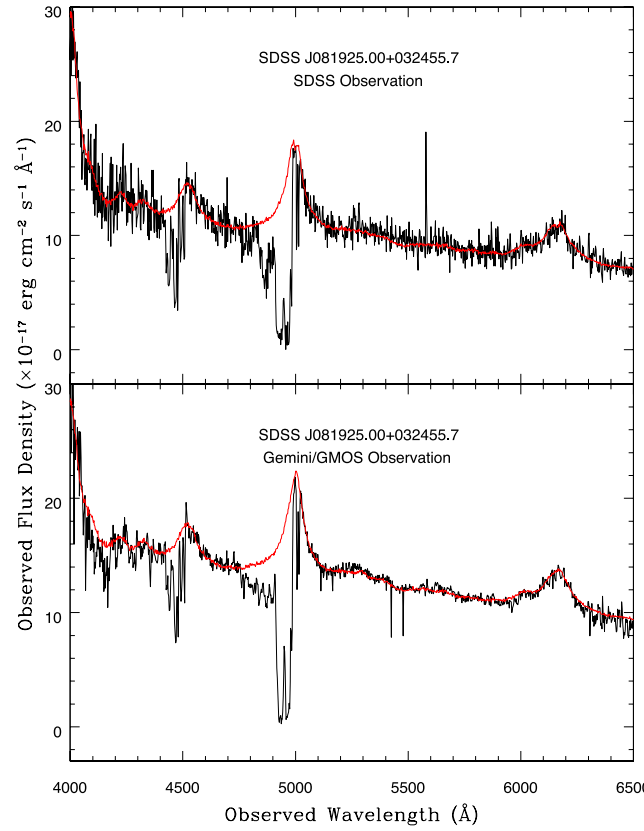

Figure 1. Top panel: example SDSS BALQSO spectrum (black) and corresponding reconstruction (red). Bottom panel: Gemini/GMOS spectrum (black) and corresponding NMF reconstruction (red) of the same object. This quasar has redshift of $z = 2.138$.

4 ANALYSIS

4.1 BAL identification

Within our BALQSO sample, individual Si IV and C IV BALs were identified using a modified BI, differing from the original BI in that a lower velocity limit of $0\,\mathrm{km\,s^{-1}}$ relative to the observed wavelength of the red doublet component of the appropriate ion emission line was used, together with an undefined upper velocity boundary (in practice no C IV absorption features are identified blueward of the Si IV emission line, corresponding to an outflow velocity of $\approx -30\,000\,\mathrm{km\,s^{-1}}$). A positive value of this modified BI for a particular absorption region categorized it as a BAL.

To carry out this procedure, the SDSS spectra and their Gemini or WHT counterparts were first resampled on to a 2.2 Å grid and smoothed using a 3 pixel boxcar smoothing algorithm to reduce the effects of noise on the determination of BAL wavelength ranges. This smoothing was applied only for the purposes of BAL identification and continuum fitting, it was not used in subsequent investigations. A power-law continuum was fitted to both the SDSS and Gemini or WHT spectra using four spectral bands in each object judged to be relatively line free. Given the limited wavelength span of the Gemini observations, a liberal approach was taken to this fitting, allowing wavelength bands in quasar rest-frame wavelength ranges of 1250–1350, 1600–1800, 1950–2050 and 21502250 Å, the only restriction being that at least one of the four bands must be in the range 1250–1350 Å and at least one must be in any of the other three. As a result, the quasar SDSSJ032832.77−070750.3 was

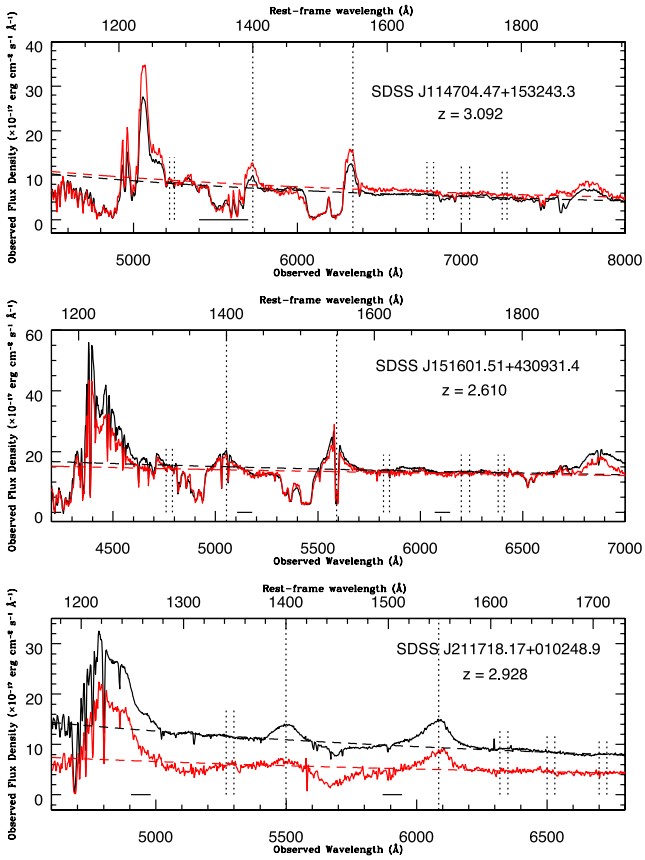

Figure 2. Power-law continuum fits to three example BALQSOs from our sample. Shown are SDSS-observed epoch 1 (red) and epoch 2 (black) spectra. Continuum models (dashed lines) are fitted to spectral bands (bracketed by short vertical dotted lines). The Si IV λ1400 and C IV λ1549 BELs are indicated by long vertical dotted lines. The top panel object's epoch 2 observations were undertaken with WHT/ISIS, the middle and lower panel objects were observed in epoch 2 with Gemini/GMOS. Black horizontal lines indicate the spectral region of the combined ISIS dichroic overlap region (top panel) or the GMOS chip gaps (middle and lower panels).

removed from our analysis as it contains no identifiable continuum regions in the 1250–1350 Å range. The modelled continuum has the form $F_\lambda = C\lambda^{-\alpha}$ where C and α were calculated using an iteratively updating procedure to minimize the chi-squared value of the fit. Three examples of BALQSO spectra and their modelled continua are shown in Fig. 2.

The SDSS spectrum and its modelled continuum for each object were examined by eye to search for regions of absorption which were plausible Si IV or C IV BAL candidates, and the upper and lower boundaries of which correspond to the points in velocity space at which the spectrum crosses the modelled continuum. These regions were then tested using a BAL identification algorithm to determine their status (BAL or non-BAL) based on the modified BI. From the total quasar sample, 38 Si IV and 59 C IV BALs were identified, these were then subjected to the variability testing stage (see Section 4.2). A total of 38 objects showed lines from both transitions while 12 contained C IV BALs only (there were no quasars in the sample in which a Si IV BAL was unaccompanied by a C IV BAL). Some BALs were identified exclusively in the epoch 2 (Gemini or WHT) spectra, these are investigated in Section 5.3 as examples of appearing BALs.

4.2 Variability testing

Prior to testing for BAL variability, each object had the higher resolution spectrum of the two epochs undergo smoothing by convolving with a Gaussian of appropriate full width at half-maximum in order to approximately degrade to the resolution of the object's other spectrum. The two spectra for each object were then resampled on to a common 2.2 Å grid for those observed with Gemini/GMOS, closely matching the maximum linear wavelength bin width of the lower resolution SDSS spectra, and 3.7 Å for those taken with WHT/ISIS, which is approximately the width of the two pixel binning in the WHT/ISIS spectra. These wavelength intervals correspond to velocity space intervals, for the redshift range covered in our sample, of between ≈85 and ≈140 km s^{-1} for the Gemini spectra and ≈140 to ≈240 km s^{-1} in the WHT/ISIS spectra (measured at a typical BAL absorber location of ≈−10 000 km s^{-1} from the C IV emission line). Small differences (a few Å) in wavelength calibration between the SDSS and Gemini or WHT spectra were removed by aligning narrow emission or absorption features within each object in the Gemini or WHT spectra to those in the SDSS spectra where a consistent difference between several of these features was obvious.

The EW of each BAL was then calculated at both epochs based on the fitted continuum used for BAL identification, propagating errors during the procedure using the SDSS and Gemini or WHT error spectra and assuming a 10 per cent continuum error. A BAL was classed as variable if the significance of the EW difference between the two epochs exceeded 2.5σ. Adopting this approach, a total of 22 Si IV and 27 C IV BALs from 35 quasars were identified as variable, giving the percentage of varying BALs as 58 per cent for Si IV and 46 per cent for C IV. This subsample includes 14 objects which contain one variable BAL of each ion, allowing for comparisons of behaviour between both types of BAL within these particular objects.

4.3 Pseudo-equivalent width

In order to investigate the variability properties of the variable BALs, we define a modified EW using equation (2), which is referred to hereafter as a 'pseudo-EW'. This quantity is normalized to the NMF reconstructions (the pseudo-continuum) as opposed to the modelled continuum EW used for BAL identification.

$$\mathrm{EW_p} = \int \frac{f_{\mathrm{cp}} - f_{\mathrm{l}}}{f_{\mathrm{cp}}}\,\mathrm{d}v, \qquad (2)$$

in this case, $\mathrm{EW_p}$ is the pseudo-EW, f_{l} is the line flux density and f_{cp} is the pseudo-continuum flux density (in each velocity bin). The depth $f_{\mathrm{cp}} - f_{\mathrm{l}}$ at each point in velocity space is therefore the difference between the absorption line flux and the sum of emission and continuum flux thought to be entering the absorber. Both transitions have doublet structures, with Si IV having a larger separation (1900 km s^{-1}) than C IV (500 km s^{-1}). This may cause Si IV BALs to be slightly wider than C IV BALs of the same intrinsic width but should not affect the validity of BAL variability measurements taken over the entire absorption line. We adopt conventions of measuring the velocities of blueshifted absorption features as negative, with pseudo-EWs being positive for regions of absorbed pseudo-continuum. However, when referring to the velocities of absorbers, terms such as greater or larger refer to the magnitude of the velocity, i.e. $|v|$.

We first translate observed wavelengths to quasar rest-frame velocities, with the laboratory wavelength of the red line of the doublet belonging to the appropriate transition defined as zero velocity. This

ensures that velocities of outflowing absorbing features will always be measured as negative at any velocity greater than zero. These zero velocities correspond to positions in wavelength space of 1402.77 Å for Si IV and 1550.77 Å for C IV. At each bin, wavelengths are converted to velocities using the relativistic Doppler shift formula:

$$\frac{v}{c} = \frac{\left(\frac{\lambda_{\rm line}}{\lambda_{\rm abs}}\right)^2 (1+z)^2 - 1}{\left(\frac{\lambda_{\rm line}}{\lambda_{\rm abs}}\right)^2 (1+z)^2 + 1}, \tag{3}$$

where $\lambda_{\rm line}$ is the rest-frame wavelength and $\lambda_{\rm abs}$ is the observed wavelength of the absorption feature. Pseudo-EW values are calculated by summing the products of pseudo-continuum-normalized depths and velocity bin widths Δv_i over the BAL velocity range $v_{\rm min}$ to $v_{\rm max}$ as follows:

$$\mathrm{EW_p} = \sum_{i=v_{\rm min}}^{v_{\rm max}} \left[\left(1 - \frac{f(i)}{f_{\rm cp}(i)}\right) \Delta v_i\right] \tag{4}$$

By utilizing the fractional error estimates in the position of the pseudo-continuum described in Section 3 as well as the SDSS, Gemini/GMOS and WHT/ISIS error spectra, a total pseudo-EW error is obtained. This consists of two functions A and B as follows:

$$A = \sum_{i=v_{\rm min}}^{v_{\rm max}} \left[\left(\frac{\sigma_f(i)}{f_{\rm cp}(i)}\right)^2 \Delta v_i^2\right] \tag{5}$$

$$B = \sum_{i=v_{\rm min}}^{v_{\rm max}} \left[\left(\frac{f(i)}{f_{\rm cp}(i)}\right)\left(\frac{\sigma_{f_{\rm cp}}(i)}{f_{\rm cp}(i)}\right) \Delta v_i\right]. \tag{6}$$

The total error in the pseudo-EW calculation is then

$$\sigma_{\mathrm{EW_p}} = \sqrt{A + B^2}. \tag{7}$$

4.4 BAL pseudo-EW variability

Following L07 (for pseudo-EW rather than continuum-based EW), we measured the fractional change in BAL pseudo-EW, $\Delta\mathrm{EW_p}/\langle\mathrm{EW_p}\rangle$, where $\Delta\mathrm{EW_p}$ is the difference in pseudo-EW and $\langle\mathrm{EW_p}\rangle$ is the average pseudo-EW across the two epochs. Fractional pseudo-EW changes are a robust method of measuring variability since they represent, for a mean value across the two epochs, a change in the BAL gas covering fraction or the fractional change, driven by ionizing continuum fluctuations, in the absorbing ion population for a non-saturated absorber. Comparisons of fractional pseudo-EW variations for an object which contains BALs from both ions and which overlap in velocity space can provide insight into outflow structure and possible contributions of ionization changes or covering fraction variations. A summary of all variable BALs, including velocity boundaries ($v_{\rm max}$ and $v_{\rm min}$), the pseudo-EWs at each epoch, the time interval between epochs in the quasar rest frame ($t_{\rm qrest}$) and the fractional pseudo-EW change $\Delta\mathrm{EW_p}/\langle\mathrm{EW}\rangle$ is presented in Table 2.

The time-scales in this study represent an intermediate epoch rest-frame separation time between the C IV short term data in L07 of a few weeks to months and the mostly longer time-scales investigated in Gibson et al. (2008, hereafter referred to as G08) and the time-scales between the Large Bright Quasar Survey (LBQS) and Hobby-Eberly Telescope (HET) observations in Gibson et al. (2010, hereafter referred to as G10). The G08 study produced results based on a three to six year quasar rest-frame epoch separation time for C IV only. G10, on the other hand, was a multi-epoch study with the longest rest-frame time period being ≈5 to 7 years additionally including the Si IV absorption region. Notably, G10 only had full spectral coverage (defined as 0 to 30 000 km s^{-1}) for Si IV in the LBQS and HET spectra and so could only provide results for the Si IV absorption region on corresponding time-scales.

Fig. 3 illustrates the fractional change in EW of BALs in our sample plotted against rest-frame time interval. A detailed investigation of the trends in variability with respect to time and other variables is reported in Section 5.

5 DISCUSSION

5.1 Trends, comparisons of C IV and Si IV properties and variability

Attempts to understand the physical mechanisms giving rise to BAL variability require an investigation into the correlations, if any, of the amplitude of variation with other properties, including the luminosity of the host quasar, elapsed rest-frame time between observations, the velocity of the bulk of the outflowing gas and BAL pseudo-EW (comprising depth, width and velocity). To achieve this, a series of Spearman rank correlation tests were carried out to determine the likelihood of dependence of $|\Delta\mathrm{EW_p}/\langle\mathrm{EW_p}\rangle|$ and $|\Delta\mathrm{EW_p}|$ on such parameters, the results of which are presented in Table 3. This was achieved by calculating the p-value for the likelihood of a null hypothesis (no underlying correlation) and subtracting it from 100 per cent probability. A correlation probability is considered highly significant if it is greater than 99 per cent. Significance values of between 95 and 99 per cent are considered plausible but no definitive conclusions are drawn from such values.

Splitting the variability dependence tests into correlations of fractional change and absolute change in $\mathrm{EW_p}$ is useful as the former could indicate that a parameter's increase or decline correlates with the fraction of outflowing gas along the line of sight affected by the variability inducing effect (possibly ionization fraction changes or changes in covering fraction). The latter may indicate that the parameter change is correlated with absolute changes in line of sight column density.

The fractional change in pseudo-EW with respect to quasar rest-frame time-scale does not show a significant correlation, with only 63 per cent confidence for C IV and 78 per cent for Si IV. This indicates that time dependence of variability amplitude is not visible in our sample over the time-scales investigated. The absolute change $\Delta\mathrm{EW_p}$ is also not correlated with rest-frame time interval in either ion. It is worth considering whether or not the rest-frame time-scales have an impact on the variability categorization of the BALs. The 35 quasars containing BALs classed as variable have a mean $t_{\rm qrest}$ of 757 d, compared with 833 d between observations for the 15 quasars containing no variable BALs. This difference is not considered to be significant as the standard deviation on the range of rest-frame time-scales of variable quasars is $\sigma_{\Delta t} = 316$ d. These findings contrast with studies on shorter and longer rest-frame time-scales (L07; G10) in which the most variable absorption features were concentrated at the longest rest-frame time intervals.

Quasars containing variable BALs have a mean luminosity of $-27.583\ M_i$ compared to a mean of $-27.307\ M_i$ for quasars containing no variable BALs. As in the case of time separation, this is not considered to be a significant difference since, for the distribution of luminosities in variable quasars, $\sigma_{\rm Lum} = 0.626\ M_i$.

SDSSJ164152.30+305851.7 is the only object in our sample which shows evidence for LoBAL absorption features. Obvious examples of these features are visible in both the WHT and SDSS observations of this object and correspond to the transitions of Al III

Table 2. Two-epoch pseudo-EWs and fractional variability of variable BALs.

Object (BAL no.)	$\Delta t_{\rm qrest}$ (d)	Ion	$v_{\rm max}$ (km s^{-1})	$v_{\rm min}$ (km s^{-1})	EW$_{\rm p1}$ (km s^{-1})	EW$_{\rm p2}$ (km s^{-1})	ΔEW$_{\rm p}/\langle$EW$_{\rm p}\rangle$
SDSSJ001025.90+005447.6	1052	C IV	−13200	−8200	2941 ± 240	3361 ± 77	0.133 ± 0.080
SDSSJ004613.54+010425.7	1282	Si IV	−20400	−3000	2986 ± 380	2245 ± 243	−0.284 ± 0.174
		C IV	−28100	−6300	5449 ± 575	4514 ± 276	−0.188 ± 0.129
SDSSJ025720.43−080322.5	1332	Si IV	−25500	−21800	1222 ± 502	1121 ± 135	−0.086 ± 0.444
SDSSJ031033.45−060957.8	1296	Si IV	−20200	−14800	673 ± 319	1253 ± 76	0.602 ± 0.355
SDSSJ031331.22−070422.8	1064	Si IV	−17100	−5600	5213 ± 178	5638 ± 53	0.078 ± 0.034
		C IV	−17400	−5800	7634 ± 199	8292 ± 47	0.083 ± 0.026
SDSSJ033223.51−065450.5	830	Si IV	−19500	−10100	3595 ± 384	3343 ± 75	−0.073 ± 0.113
SDSSJ035749.11−061121.9	1328	C IV	−13600	−7000	2394 ± 178	656 ± 102	−1.139 ± 0.155
SDSSJ073535.44+374450.4	994	Si IV	−19800	−5000	3729 ± 238	5074 ± 87	0.305 ± 0.058
		C IV	−28000	−7500	7716 ± 355	8978 ± 99	0.151 ± 0.044
SDSSJ081823.46+484910.8	1252	C IV	−14100	−5300	3703 ± 488	2512 ± 411	−0.383 ± 0.209
SDSSJ081925.00+032455.7	1032	Si IV	−9000	−4000	1686 ± 148	1109 ± 44	−0.412 ± 0.113
SDSSJ083718.63+482806.1	804	Si IV	−16100	−4500	5210 ± 177	6132 ± 92	0.163 ± 0.035
SDSSJ084408.29+423226.9	775	Si IV	−17800	−5200	2825 ± 145	3364 ± 80	0.174 ± 0.054
		C IV	−21300	−4700	5712 ± 436	6475 ± 86	0.125 ± 0.073
SDSSJ085006.08+072959.0	819	C IV	−27300	−13900	1313 ± 188	0 ± 113	−2.000 ± 0.472
SDSSJ085104.05+051539.8	446	Si IV	−12600	−5300	2112 ± 176	3662 ± 32	0.537 ± 0.064
		C IV	−11300	−4000	5578 ± 87	5814 ± 21	0.041 ± 0.016
SDSSJ092639.34+383656.7	912	C IV	−22800	−8600	3772 ± 645	2841 ± 185	−0.282 ± 0.205
SDSSJ093251.98+023727.0	1272	Si IV	−30700	−6300	1086 ± 901	2536 ± 648	0.801 ± 0.660
		C IV	−29400	−11000	6211 ± 475	7443 ± 179	0.180 ± 0.075
SDSSJ100312.63+402505.6	606	Si IV	−13400	−7200	2503 ± 277	2857 ± 72	0.132 ± 0.107
SDSSJ101056.68+355833.3	687	C IV	−13100	−3400	6407 ± 149	6333 ± 127	−0.012 ± 0.031
SDSSJ104059.79+055524.4	963	Si IV	−15600	−4500	2295 ± 396	4202 ± 55	0.587 ± 0.128
SDSSJ110041.19+003631.9	1346	Si IV	−17000	−5500	2909 ± 435	633 ± 185	−1.285 ± 0.317
		C IV	−22100	−5000	7029 ± 505	3246 ± 233	−0.736 ± 0.115
SDSSJ110339.90+011928.5	1173	Si IV	−10800	−4800	1909 ± 400	2871 ± 128	0.403 ± 0.179
SDSSJ112733.69+343008.8	436	C IV	−19500	−11100	2377 ± 418	2857 ± 129	0.184 ± 0.168
SDSSJ113831.42+351725.3[a]	360	Si IV	−14100	−1600	4381 ± 621	1501 ± 180	−0.979 ± 0.245
		C IV	−20900	−1700	8905 ± 782	4764 ± 236	−0.606 ± 0.125
SDSSJ114704.47+153243.3[a]	303	Si IV	−20600	−3200	7354 ± 403	7157 ± 145	−0.027 ± 0.059
		C IV	−27300	−3200	10323 ± 620	7918 ± 200	−0.264 ± 0.072
SDSSJ134458.82+483457.5[a]	615	C IV	−21100	−7100	2688 ± 1058	5493 ± 319	0.686 ± 0.288
SDSSJ142244.45+382330.6	311	C IV	−16500	−7400	2542 ± 239	3808 ± 60	0.399 ± 0.079
SDSSJ143604.64+350428.5	616	Si IV	−20600	−10800	4342 ± 663	3837 ± 238	−0.124 ± 0.172
		C IV	−16800	−7000	7828 ± 557	5146 ± 183	−0.413 ± 0.092
SDSSJ151601.51+430931.4	691	Si IV	−15300	−5700	3633 ± 196	4169 ± 85	0.138 ± 0.055
		C IV	−25800	−4600	5712 ± 380	6755 ± 122	0.167 ± 0.064
SDSSJ162657.47+405848.0[a]	551	C IV	−13100	−2500	5884 ± 238	4886 ± 107	−0.185 ± 0.049
SDSSJ164152.30+305851.7[a]	611	Si IV	−30400	−1800	26259 ± 1468[b]	26519 ± 212[b]	0.010 ± 0.056[b]
		C IV	−27600	−1800	13166 ± 1166	13886 ± 212	0.053 ± 0.088
SDSSJ210436.62−070738.3	1080	C IV	−23500	−9800	2674 ± 462	5922 ± 58	0.756 ± 0.116
SDSSJ211718.17+010248.9	860	Si IV	−27700	−13100	1931 ± 512	292 ± 121	−1.475 ± 0.588
		C IV	−25800	−15100	3348 ± 372	664 ± 85	−1.338 ± 0.229
SDSSJ212412.60+095923.3[a]	737	Si IV	−13300	−3300	1054 ± 966	227 ± 450	−1.291 ± 1.981
		C IV	−14000	−2900	6299 ± 515	3872 ± 434	−0.477 ± 0.136
SDSSJ213138.93−070013.3	1188	C IV	−27400	−3800	5368 ± 1185	5697 ± 557	0.059 ± 0.237
SDSSJ222505.28−084542.7	1176	C IV	−26900	−7500	4464 ± 1165	2380 ± 467	−0.609 ± 0.384

[a]These objects were observed using WHT/ISIS, unmarked objects were observed using Gemini/GMOS.
[b]May include contamination from C II LoBAL.
Outflow velocities are rounded to the nearest 100 km s^{-1} as the error in velocity width is $\approx$ 200 km s^{-1}.
EW$_{\rm p1}$ and EW$_{\rm p2}$ denote pseudo-EW for earlier and later epochs, respectively.

at 1860 Å and Mg II at 2798 Å. In addition to these, in Hall et al. (2002) a rarer LoBAL resulting from the C II transition at 1334 Å was found in several LoBAL QSOs. A measurement of the average pseudo-EW between −1800 and −30 400 km s^{-1} from the Si IV emission line centre gives an exceptionally large value of $\langle$EW$_{\rm p}\rangle$ = 26 389 ± 742 km s^{-1}, several times that of the next strongest BAL in the Si IV sample. It therefore seems very plausible that this measurement is contaminated by additional C II LoBAL absorption in the Si IV BAL absorption range, given that the centre of the C II emission line is located approximately −15 000 km s^{-1} from the centre of the Si IV emission line. Further evidence for the possible existence of such absorption is provided by the fact that the Al III LoBAL spans a velocity range of approximately 0 to −14 000 km s^{-1}, providing the likely position of any C II absorption (indicated in Fig. 4). For these

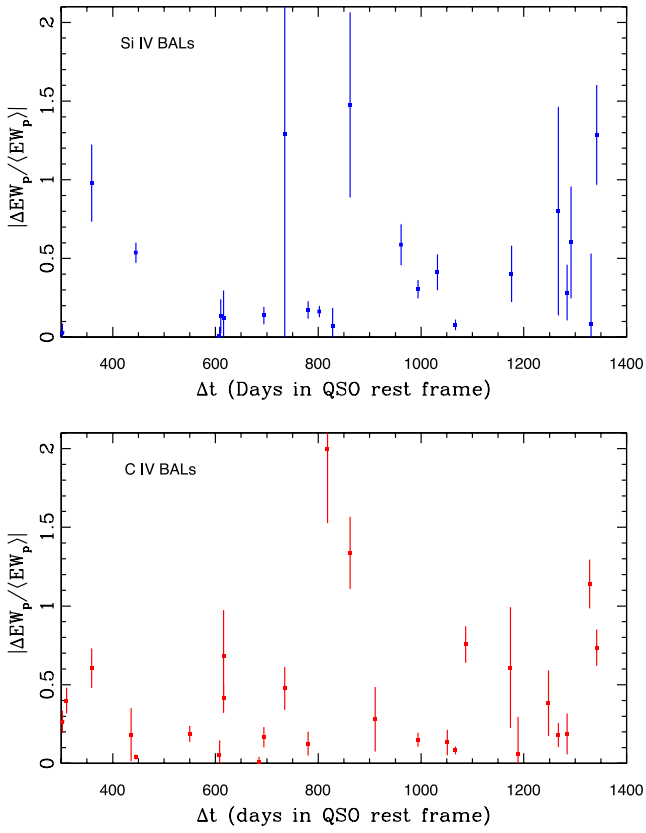

Figure 3. Magnitude of fractional change in pseudo-EW against quasar rest-frame time interval between epochs for Si IV (upper panel) and C IV (lower panel).

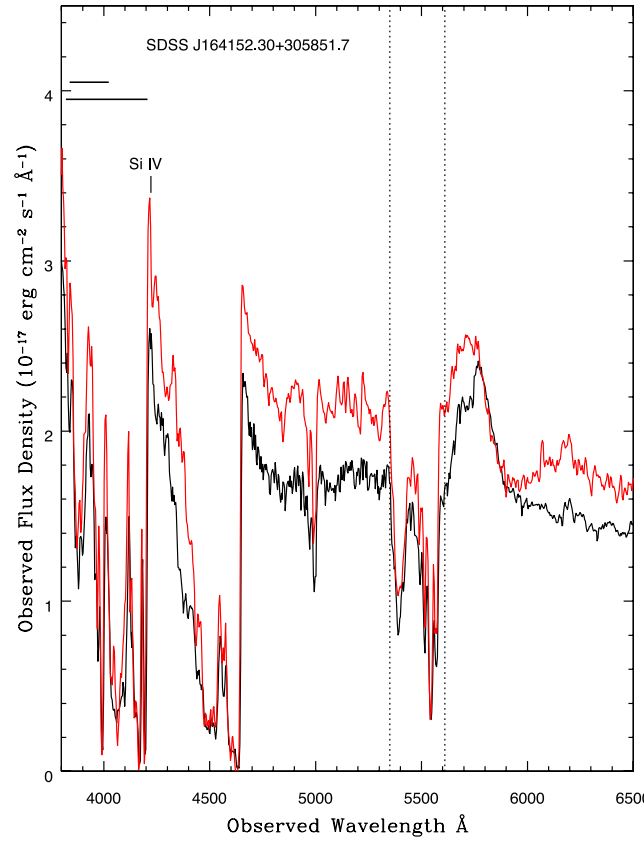

Figure 4. WHT/ISIS spectrum (black) and Gemini/GMOS spectrum (red) of the LoBAL quasar SDSS J164152.30+305851.7. Dotted vertical lines indicate the extent of Al III LoBAL absorption (from 0 to approximately −14 000 km s^{-1}). The Si IV emission line is also labelled. The lower thick horizontal black line indicates the range of BAL absorption measured blueward of the Si IV emission line, while the upper thick horizontal black line indicates the possible location of C II LoBAL absorption based on the extent of the Al III absorption.

reasons, the Si IV BAL from J164152.30+305851.7 is not included in the tests for dependence on average pseudo-EW, or its component quantities of depth and width.

A significant correlation is not observed in the $|\Delta EW_p|$ versus $\langle EW_p \rangle$ relationship, which the Spearman rank test gives as 72 per cent confidence for Si IV and 41 per cent for C IV. The value of $\langle EW_p \rangle$ can be split into two more fundamental properties, one being the velocity width (V_{width}) of the BAL, corresponding to the difference in velocity between the upper and lower boundaries of the BAL trough, the other being the depth ($\langle B_{depth} \rangle$), defined as the mean pseudo-continuum-normalized depth across the BAL trough averaged between the two epochs. Our test of $|\Delta EW_p/\langle EW_p \rangle|$ versus V_{width} does not give a significant correlation for either Si IV or C IV (significance of 40 per cent for both ions). This is in stark contrast with the strong inverse correlation found for the $|\Delta EW_p/\langle EW_p \rangle|$ versus $\langle B_{depth} \rangle$ dependence, which the Spearman rank test reveals to be >99.99 per cent for the Si IV sample and 99.95 per cent for the C IV sample, with the negative sign of ρ indicating an inverse scaling (see Fig. 5). However, this result is likely to be due to the fact that $\langle EW_p \rangle$ shows a strong positive correlation with $\langle B_{depth} \rangle$ in both Si IV (99.97 per cent significance) and C IV (99.93 per cent significance).

Table 3. Results of Spearman rank correlation tests.

Comparison	Si IV confidence (sign of ρ)	C IV confidence (sign of ρ)
$\|\Delta EW_p\|$ versus $\langle EW_p \rangle$	72 per cent[a] (−)	41 per cent (−)
$\|\Delta EW_p/\langle EW_p \rangle\|$ versus B_{vel}	78 per cent (−)	93 per cent (+)
$\|\Delta EW_p\|$ versus B_{vel}	92 per cent (−)	71 per cent (+)
$\|\Delta EW_p/\langle EW_p \rangle\|$ versus $\langle B_{depth} \rangle$	>99.99 per cent[a] (−)	99.95 per cent (−)
$\|\Delta EW_p\|$ versus $\langle B_{depth} \rangle$	98 per cent[a] (−)	93 per cent (−)
$\|\Delta EW_p/\langle EW_p \rangle\|$ versus M_i	61 per cent (+)	93 per cent (+)
$\|\Delta EW_p\|$ versus M_i	6 per cent (−)	97 per cent (+)
$\|\Delta EW_p/\langle EW_p \rangle\|$ versus t_{qrest}	78 per cent (+)	63 per cent (+)
$\|\Delta EW_p\|$ versus t_{qrest}	51 per cent (+)	15 per cent (+)
$\|\Delta EW_p/\langle EW_p \rangle\|$ versus V_{width}	40 per cent[a] (+)	40 per cent (−)
$\|\Delta EW_p\|$ versus V_{width}	83 per cent[a] (+)	58 per cent (+)

[a]The unusual Si IV $\langle EW_p \rangle$ measurement for J164152.30+305851.7 is not included in this test.

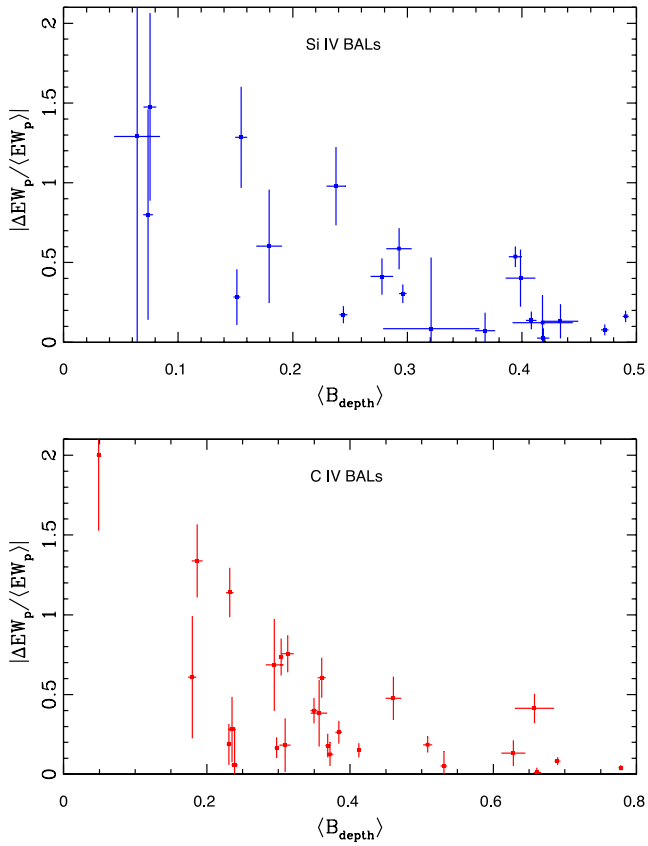

Figure 5. Fractional pseudo-EW variability for Si IV BALs (top panel) and C IV BALs (bottom panel) versus average mean normalized BAL depth across the two epochs. Outlying Si IV BAL measurement from J164152.30+305851.7 is not included.

Since the fractional pseudo-EW measure incorporates $\langle EW_p\rangle$ as the denominator, such a correlation is not inferred to represent anything physical. Correlation probability is possibly significant (98 per cent) in the $|\Delta EW_p|$ versus B_{depth} relationship for Si IV BALs but not so in the C IV sample (93 per cent), with negative ρ in both cases. This is similar to the findings of G10 for C IV BALs, which found no correlation between the absolute change in absorption strength in velocity ranges which varied and the depth of those regions. There is no discernible correlation between $|\Delta EW_p|$ and V_{width} (83 per cent correlation confidence for Si IV and 58 per cent for C IV). Previous work comparing variability to velocity width is minimal, although Filiz Ak et al. (2012) found tentative evidence that relatively narrow C IV BALs are more likely to undergo disappearance than wider BALs.

For this study, the BAL velocity (B_{vel}) is defined as the velocity of the depth centroid of the BAL feature, giving the best estimate of the value for the column density weighted mean of the velocity of the outflowing gas. A study of the dependence of variability amplitude on velocity across a range of velocity bins in a sample of C IV BALs in Capellupo et al. (2011) showed a relationship of strengthening variability with increased velocity. The test for the correlation of $|\Delta EW_p/\langle EW_p\rangle|$ on B_{vel} in our data set returns a probability of 78 per cent for Si IV and 93 per cent for C IV, implying that there is no discernible correlation. Although this is not exactly the same type of study as in Capellupo et al. (2011) since our work reports on statistics for the whole BAL features rather than portions thereof, this may suggest a contradiction with those previously reported results. For the $|\Delta EW_p|$ versus B_{vel} relationship, correlation significances of 92 per cent for Si IV BALs and 71 per cent for C IV BALs are found.

The dependence or otherwise of the host quasar luminosity on BAL variability can shed light on the contribution of ionization fraction changes to the variability, as it is a general property of quasars that emission line variability, which is known to be driven by ionization continuum variations, has an inverse dependence on host luminosity (Vanden Berk et al. 2004). Luminosity is defined in terms of the SDSS *i*-band absolute magnitude (M_i) as listed in Shen et al. (2011). There is no strong evidence in this sample, in either C IV or Si IV BALs, of a correlation in the $|\Delta EW_p/\langle EW_p\rangle|$ versus M_i relationship, given correlation probabilities of 93 and 61 per cent, respectively. The Spearman rank test also gives a confidence of 6 per cent for Si IV and 97 per cent for C IV correlation with respect to $|\Delta EW_p|$ versus M_i, which, given a positive value of ρ, may indicate an inverse scaling between the absolute variability and luminosity for C IV BALs. BAL variability dependence on host quasar luminosity has not been extensively studied, however, Filiz Ak et al. (2012) reported no correlation between quasar luminosity and the rate of C IV BAL disappearance.

5.1.1 Quasars containing both Si IV and C IV variable BALs

An interesting subsample of quasars containing variable BALs is that which contains examples of both Si IV and C IV, allowing direct comparison of the behaviour of these absorption features within the same objects. There are 14 such quasars in our sample, each consisting of one BAL from each ion. Two notable facts are apparent in this subsample, namely (1) for any given quasar, both BALs change in the same direction (as has been noted previously in Capellupo et al. 2012) and (2) when considering the velocity range over which the BALs span, there is a considerable overlap between the C IV and Si IV outflows. This suggests that the same outflowing structure is responsible for such BALs and that the dominant variability mechanism is the same in each case.

Comparisons of the average values of several BAL parameters between each ion can provide an insight into the likely physical mechanisms leading to variability. For example, if the outflows of one ion were found to be at a significantly higher mean velocity than that of the other ion then, following the model of Elvis (2000), this would provide evidence for this ion having a greater density than the other at positions closer to the origin of the outflow. Table 4 provides mean values of several properties in the dual ion variable BAL subsample, while Fig. 6 displays the spectra of these objects.

Table 4. Mean BAL properties for quasars containing variable BALs from both ions.

Property	Si IV mean	C IV mean
B_{vel}	$-13181 \pm 55\,km\,s^{-1}$	$-11762 \pm 53\,km\,s^{-1}$
$B_{vel}{}^a$	$-12271 \pm 56\,km\,s^{-1}$	$-11880 \pm 54\,km\,s^{-1}$
$\langle EW_p\rangle$	$4881 \pm 92\,km\,s^{-1}$	$6738 \pm 80\,km\,s^{-1}$
$\langle EW_p\rangle^a$	$3226 \pm 80\,km\,s^{-1}$	$6216 \pm 72\,km\,s^{-1}$
$\lvert\Delta EW_p/\langle EW_p\rangle\rvert$	0.536 ± 0.159	0.345 ± 0.028
$\lvert\Delta EW_p/\langle EW_p\rangle\rvert^a$	0.577 ± 0.171	0.367 ± 0.030
V_{width}	$14439 \pm 111\,km\,s^{-1}$	$16812 \pm 107\,km\,s^{-1}$
$V_{width}{}^a$	$13345 \pm 113\,km\,s^{-1}$	$16120 \pm 109\,km\,s^{-1}$
$\langle B_{depth}\rangle$	0.308 ± 0.003	0.431 ± 0.002
$\langle B_{depth}\rangle^a$	0.262 ± 0.003	0.423 ± 0.003*

[a]SDSSJ164152.30+305851.7 excluded.

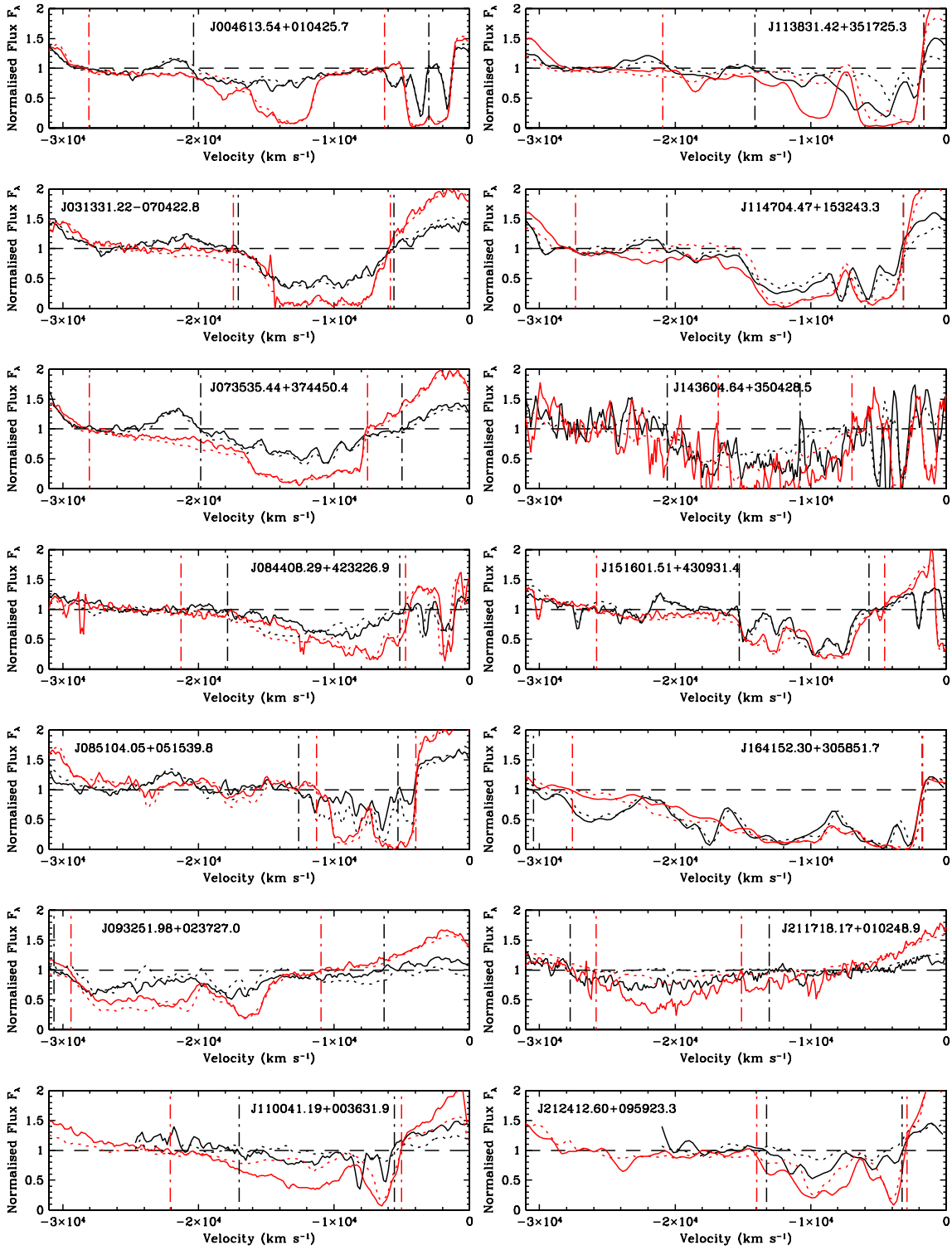

Figure 6. Behaviour of Si IV (black) and C IV (red) BAL regions plotted in concurrent velocity space for each of the dual ion variable BAL quasar sample. Spectra are smoothed using a 3 pixel boxcar smoothing for clarity. Solid lines represent the SDSS spectra while dotted lines represent the Gemini/WHT spectra. Vertical dash–dotted lines represent the BAL boundaries. A can be seen, the overlap region forms the majority of the width of both BALs in every case.

This sample includes the LoBAL quasar SDSSJ164152.30+305851.7 which contains a Si IV BAL region of exceptional large average pseudo-EW of $\langle EW_p \rangle = 26389 \pm 742\,km\,s^{-1}$, which is not matched by a similarly large C IV BAL and may be due to C II absorption contaminating the measurement. Table 4 therefore includes a duplicate set of comparisons from which SDSSJ164152.30+305851.7 is excluded. If all 14 quasars are taken into account, the mean BAL velocity of Si IV is larger than that of C IV by $\approx$1419 km s^{-1}, however, this reduces to a difference of $<$400 km s^{-1}, about twice the typical BAL velocity error, in the

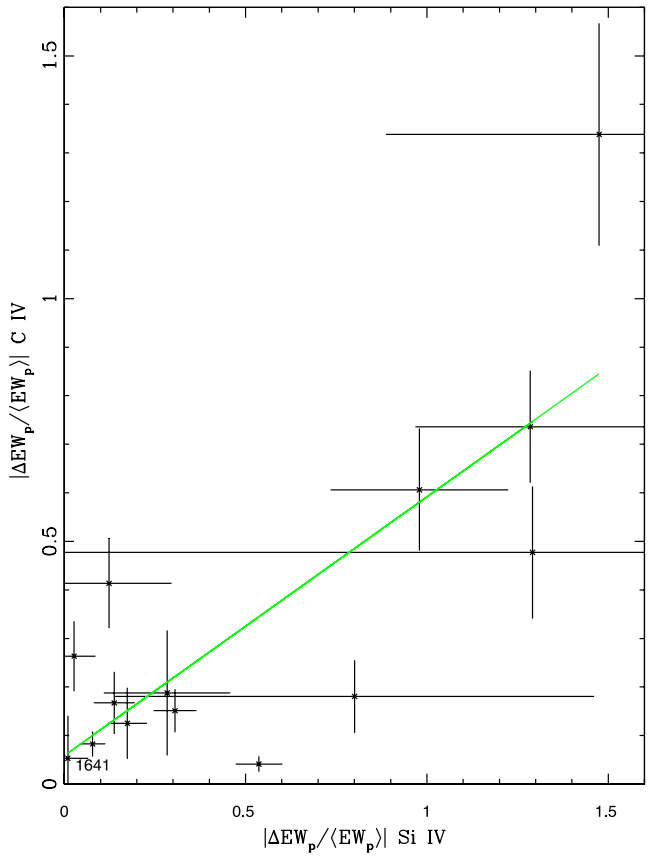

Figure 7. Fractional change in pseudo-EW for C IV (vertical axis) and Si IV (horizontal axis). The green line represents a least-squares fit to the data.

13 quasar sample. This difference is therefore considered to be consistent with zero. The mean epoch averaged pseudo-EW is larger in C IV than in Si IV by 38 per cent, which increases dramatically to 93 per cent in the 13 quasar sample where the apparent large Si IV BAL from SDSSJ164152.30+305851.7 is excluded. This difference is mainly explained by the fact that C IV BALs are on average 40 per cent deeper (61 per cent in the 13 quasar sample) than Si IV. However, there is also a difference in velocity width, with the mean value for C IV being $\approx$2400 km s^{-1} larger, or $\approx$2800 km s^{-1} larger without the LoBAL quasar, than that for Si IV. Also, the Si IV BALs show a 55 per cent (57 per cent for the 13 quasar sample) stronger mean fractional pseudo-EW variability than C IV.

To determine what relationship, if any, exists between the variability of all the Si IV and C IV BALs in this quasar subsample, a Spearman rank test was carried out to determine the significance of a correlation between the Si IV and C IV values of $|\Delta EW_p/\langle EW_p\rangle|$. This reveals a probability of 98 per cent of correlation, just below the threshold of 99 per cent for strong significance. The test was also performed on the dependence of $|\Delta EW_p|$ of Si IV to that of C IV, revealing a probability of correlation of 91 per cent, too low to be considered significant. This relationship between the fractional changes in BAL pseudo-EW of the two ions is illustrated in Fig. 7 and shows that a least-squares fit line closely matches eight of the data points, including that of the LoBAL SDSSJ164152.30+305851.7 (marked '1641' in the plot). No properties of the BALs nor their host quasars were found that distinguished those which fell relatively close to the best-fitting line from those which did not.

In previous work (G10), a significant correlation was found (>99 per cent) between the absolute fractional change in the total pseudo-EW in the absorption regions of C IV and Si IV (defined in that study as all spectral bins spanning 0 to −30 000 km s^{-1} from the rest wavelength of the red doublet component, as opposed to only the identified BAL regions used in this study) of nine quasars over rest-frame time intervals of $\approx$5–7 years. This high correlation depended on the exclusion of one outlying quasar, 1235+1453, which displayed a strong variability in the C IV BAL, but virtually no change in the Si IV BAL and showed a very blue continuum component which declines over subsequent observations and is not absorbed by the BAL region. A fitted line to this data (see fig. 12 in G10) gave a gradient of 1.44 ± 0.45 and intercept −0.05 ± 0.019 for the Si IV versus C IV pseudo-EW. Equivalent values from our data give a gradient of 1.88 and intercept of −0.11, well within the margin of error for both quantities.

5.2 Quasars containing both variable and non-variable BALs

Of the 35 quasars containing at least one variable BAL, 15 also contained at least one non-variable BAL. Included in these are 8 containing a varying Si IV BAL and a non-varying C IV BAL, 5 containing a varying C IV BAL and a non-varying Si IV BAL and 5 containing a varying C IV BAL while a second C IV BAL did not vary. These instances are recorded in Table 5.

The 13 showing variability in one ion and no variability in the other are particularly interesting as it is possible to investigate the extent, if any, of the velocity overlap. The spectral extent in velocity space of the BALs is illustrated in Fig. 8.

There is no velocity overlap at all between the two BALs in J142244.45+382330.6 (bottom-right panel), while J134458.82+483457.5 (top-left panel) and J025720.43−080322.5 (middle-left panel) only show minimal overlap. The BALs in quasar J162657.47+405848.0 overlap but the region where the C IV BAL varies is largely non-overlapped. Of the 9 remaining quasars showing substantial velocity overlap in variable regions, 2 show C IV variation without Si IV variation while the remaining 7 showed the reverse situation. A lack of velocity space overlap in these objects suggests that their BALs are not part of the same outflow, see Section 6.2 for a further discussion.

5.3 BAL appearance and disappearance

There is now a substantial body of evidence showing spectral regions containing BALs transforming into regions where absorption features no longer meet the BAL definition. This can occur for both HiBALs and LoBALs (Hamann et al. 2008; Vivek et al. 2012) and are referred to as cases of disappearing BALs. Disappearing BALs can transform into either spectral regions of no absorption or weaker absorption features. Such weaker features include mini-BALs (Capellupo et al. 2012; Rodriguez Hidalgo et al. 2012) and NALs. Other BALs have been observed to emerge from apparently absorption free regions or from the types of aforementioned weaker absorption features and are referred to as appearing BALs. For this study, such events are confirmed only if the following two criteria are met, that disappearance or appearance takes place based on the BAL definition outlined in Section 4.1 and the significance meets the 2.5σ variability criteria (also described in Section 4.1). Unlike in previous sections of this paper, we allow identification of BALs from second epoch data alone in order to record instances of BAL appearance. Table 6 provides a list of disappearing and appearing BALs along with their strengths as measured by the pseudo-EW at epochs 1 and 2.

Table 5. Quasars containing both variable and non-variable BALs.

Object name	Varying Si IV+non-varying C IV	Varying C IV+non-varying Si IV	Varying C IV+non-varying CIV
SDSSJ001025.90+005447.6	No	Yes	Yes
SDSSJ004613.54+010425.7	No	No	Yes
SDSSJ025720.43−080322.5	Yes	No	No
SDSSJ031033.45−060957.8	Yes	No	No
SDSSJ033223.51−065450.5	Yes	No	No
SDSSJ081925.00+032455.7	Yes	No	No
SDSSJ083718.63+482806.1	Yes	No	No
SDSSJ100312.63+402505.6	Yes	No	No
SDSSJ101056.68+355833.3	No	Yes	No
SDSSJ104059.79+055524.4	Yes	No	No
SDSSJ110339.90+011928.5	Yes	No	No
SDSSJ134458.82+483457.5	No	Yes	Yes
SDSSJ142244.45+382330.6	No	Yes	Yes
SDSSJ162657.47+405848.0	No	Yes	No
SDSSJ210436.62−070738.3	No	No	Yes

We note the appearance of a C IV BAL in the spectrum of J112733.69+343008.8 from a spectral region that was formerly almost entirely above continuum level (see Fig. 9). This case is noteworthy as it is accompanied by the emergence of a Si IV BAL where previously there had been a few non-contiguous NALs. This is more of a merging than a strengthening as the change in pseudo-EW is consistent with zero. Although the width of the Si IV BAL is 16 100 km s^{-1}, much wider than the 2600 km s^{-1} C IV BAL, the deepest feature of the Si IV BAL largely occupies the same velocity range, while most of the Si IV BAL outside this range is so shallow as to be consistent with zero absorption. It is therefore likely that these two BALs represent absorption from the same outflow. In addition, this object hosts a second faster C IV BAL with a minimum velocity ≈1200 km s^{-1} greater than that of the maximum velocity of the appearing C IV BAL. Although this velocity separation suggests that it is not part of the same outflow as the emerging C IV BAL, it also undergoes a strengthening of $\Delta EW_p = 480 \pm 437$ km s^{-1}.

In the case of J100021.72+035116.5 two Si IV BALs of similar strength appear to emerge in an almost contiguous absorption region saved for a small break of ≈200 km s^{-1} which protrudes above the continuum and separates them (see Fig. 10). The lower velocity BAL of the two contained a mini-BAL at epoch 1 which strengthened significantly to become a BAL of width 3300 km s^{-1}. The higher velocity BAL emerged from a spectral region having pseudo-EW consistent with zero (99 ± 209 km s^{-1}). At the second epoch the same spectral region contained a BAL of width 4000 km s^{-1}. The lower velocity Si IV BAL coexists with a C IV BAL at a mostly overlapping velocity range. Interestingly this C IV BAL does not show significant variability. There is also a second C IV BAL at higher velocity of width 9800 km s^{-1} which overlaps most of the velocity range (≈3000 km s^{-1}) of the higher velocity Si IV BAL. This C IV BAL also does not show significant variability. However, only shallow parts of this BAL are in the overlapping region.

As the disappearing BALs all meet the variability criteria and are present in the first epoch, they are also listed in Table 2. Fig. 11 illustrates the spectra of these features across the two epochs for all instances of BAL disappearance.

In Filiz Ak et al. (2012), 21 examples of C IV BAL disappearance were reported from a sample of 582 BALQSOs on similar rest-frame time-scales to this investigation (1.1 to 3.9 years). We observe one case of such behaviour of a C IV BAL from our sample, that of the disappearance from J085006.08+072959.0 where the BAL appears to have transformed into a narrower and significantly weaker feature (≈4000 km s^{-1} width without being sub-90 per cent of continuum over a contiguous 2000 km s^{-1}) which meets the criteria for a mini-BAL. This changes the quasar's categorization from BALQSO to non-BALQSO as there are no other BALs present for either ion in the second epoch. Over the entire velocity range formerly occupied by the BAL, the pseudo-EW has declined to a level consistent with zero. The solitary C IV BAL disappearance in one quasar from our sample of 50 objects containing 59 C IV BALs gives a BAL disappearance rate of 1.7 per cent and a fraction of quasars hosting C IV BALs undergoing an episode of disappearance of 2.5 per cent. This is consistent with the statistics reported in Filiz Ak et al. (2012) of ≈2.3 per cent of C IV BALs disappearing and ≈3.3 per cent of BALQSOs hosting one of these disappearances over similar rest-frame time-scales.

Disappearance of the Si IV BAL occurs in J211718.17+010248.9, with the remaining absorption reduced to a few narrow and weak absorption features. This is accompanied by the strong reduction in strength of the C IV line in this object by $\Delta EW_p = -2684 \pm 382$ km s^{-1}, with which it overlaps almost entirely in velocity range (this can be seen by comparing the spectra of J211718.17+010248.9 in Figs 11 to 6). We also report the disappearance of a weak Si IV BAL in J212412.60+095923.3, reducing the total absorption in the region to a pseudo-EW within 1σ of zero. The weakness of this feature is highlighted by the fact that, as in the case of the appearing Si IV BAL in J112733.69+343008.8, the error on the change in pseudo-EW makes it consistent with zero. Again this was accompanied by a strong reduction in the strength of the C IV feature of $\Delta EW_p = -2427 \pm 673$ km s^{-1} over a very similar velocity range (again compare Fig. 11 with Fig. 6). The fraction of Si IV BALs that disappear is 2 out of 38, giving a disappearance rate of 5.26 per cent. This is also the disappearance rate per Si IV hosting quasar since no object hosts more than one Si IV BAL.

5.4 Evidence of a covered continuum and uncovered BLR

It was reported in Arav et al. (1999) that a section ≈1700 km s^{-1} wide in the profile of the C IV BAL in FIRST J160354.2+300209 showed evidence of being due to an outflow which almost entirely absorbed the continuum while leaving the overlapping C IV BEL unabsorbed. This was thought to be due to an optically thick absorber which completely covers the continuum emitting region while leaving the much larger broad line region (BLR) unobscured. We look for this same effect in our sample by seeking out those

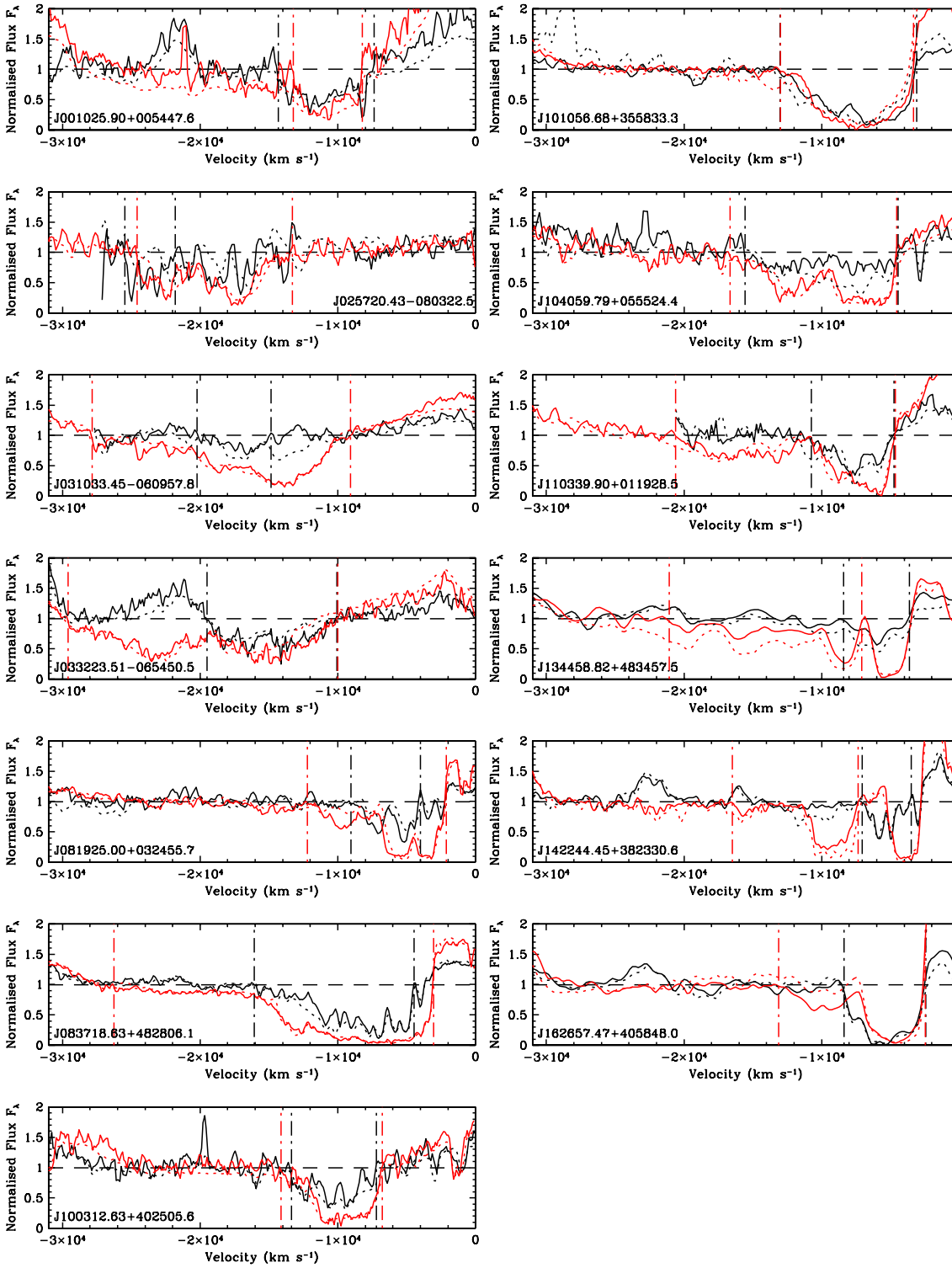

Figure 8. Behaviour of Si IV (black) and C IV (red) BAL regions plotted in concurrent velocity space for each of the one ion variable and one ion non-variable quasar sample (from Table 5). Spectra are smoothed using a 3-pixel boxcar smoothing for clarity. Solid lines represent the SDSS spectra while dotted lines represent the Gemini/WHT spectra. Vertical dash–dotted lines represent the BAL boundaries. A gap occurs between $-12\,500$ km s^{-1} and -9200 km s^{-1} in the SDSS spectrum of Si IV in J025720.43−080322.5 due to an unknown instrumental issue.

C IV troughs where the base overlaps with the emission line velocity range and shows a gradient consistent with the emission line profile. To create a model profile of the uncovered emission, an appropriate fraction of the continuum (up to 100 per cent) was selected to be subtracted from the original reconstructed emission, whose value was determined by finding the fraction which minimized χ^2 between the observed spectrum and this model over a velocity range where the trough profile appeared to be similar to the

Table 6. Appearing (upper panel) and disappearing (lower panel) BALs. Total number of BALs in each quasar for each ion is given by $T_{\rm no.}$. Pseudo-EWs are calculated over the velocity ranges which the single epoch BALs occupy.

Object	Ion	EW_{p1} (km s^{-1})	EW_{p2} (km s^{-1})	ΔEW_p (km s^{-1})	$T_{\rm no.}$ (Si IV/C IV)
SDSSJ100021.72+035116.5	Si IV	589 ± 159	1509 ± 99	920 ± 187	2/2
SDSSJ100021.72+035116.5	Si IV	99 ± 209	1229 ± 123	1130 ± 243	2/2
SDSSJ112733.69+343008.8	Si IV	1004 ± 717	1549 ± 295	545 ± 775	1/2
SDSSJ112733.69+343008.8	C IV	0 ± 177	787 ± 52	787 ± 184	1/2
SDSSJ085006.08+072959.0	C IV	1313 ± 188	0 ± 113	−1313 ± 219	0/1
SDSSJ211718.17+010248.9	Si IV	1931 ± 512	292 ± 121	−1639 ± 526	1/1
SDSSJ212412.60+095923.3	Si IV	1054 ± 966	227 ± 450	−827 ± 1065	1/1

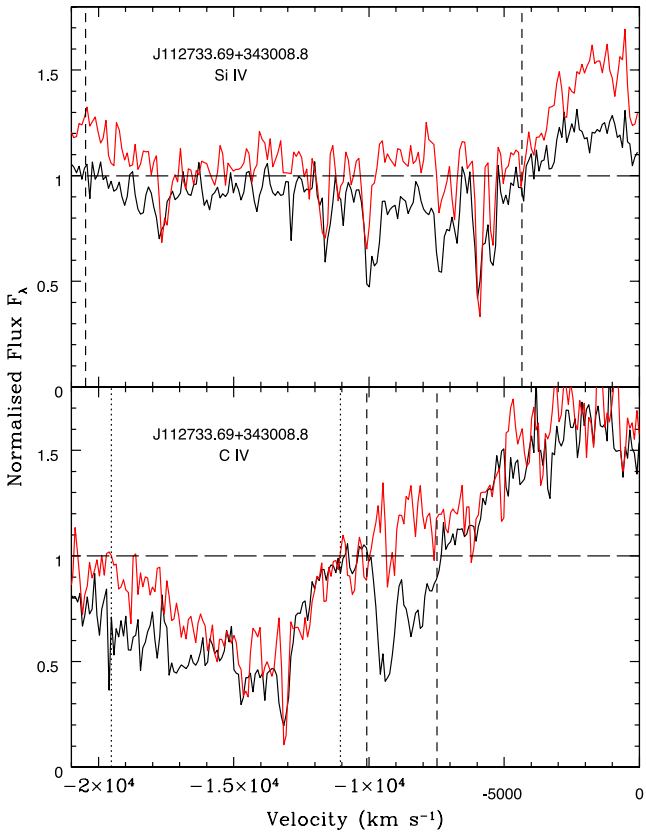

Figure 9. Appearance of a Si IV BAL (top panel) and a C IV BAL (bottom panel) in the quasar SDSSJ112733.69+343008.8 with SDSS observation in red and Gemini/GMOS observation in black. Vertical dashed lines indicate boundaries of appearing BALs. Vertical dotted lines indicate the position of the second C IV BAL which undergoes strengthening.

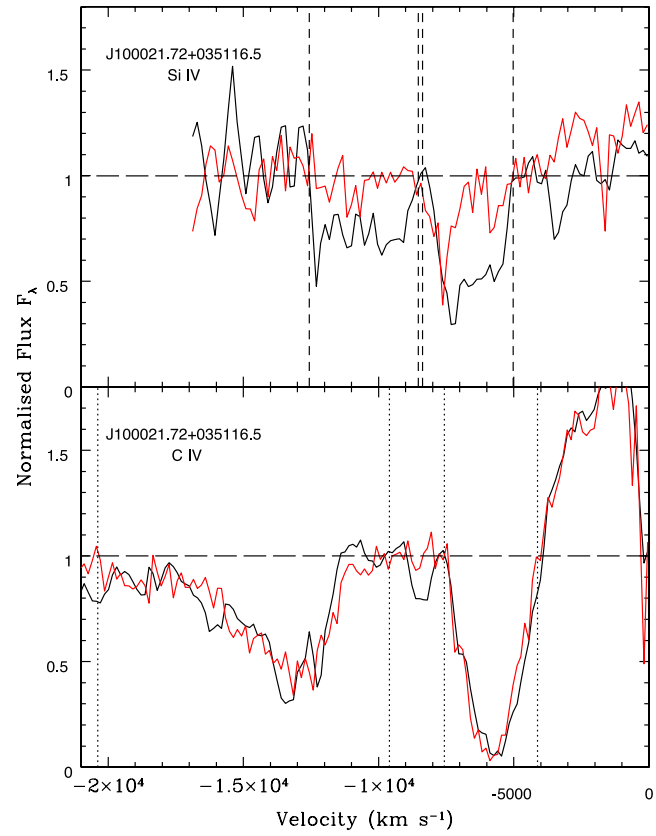

Figure 10. Appearance of a Si IV BAL (top panel) and a C IV BAL (bottom panel) in the quasar SDSSJ100021.72+035116.5 with SDSS observation in red and Gemini/GMOS observation in black. Vertical dashed lines indicate boundaries of appearing BALs. Vertical dotted lines indicate the position of the C IV BALs which do not meet the variability criteria.

continuum absorbed emission profile. A good match was found in 5 C IV BALs, one in each of five quasars. Details for these C IV BALs is provided in Table 7, while their spectra are illustrated in Fig. 12. None of these objects showed evidence for the same effect in Si IV BALs.

When considering the variation between the two epochs, we find no strong evidence for a change in the covering fraction over these velocity ranges. It is also notable that 4 of the 5 C IV BALs are not variable. Only the BAL in SDSSJ073535.44+374450.4 meets the variability criteria, however, within the velocity range over which the BAL profile follows the emission line profile, this feature also shows no variability.

5.5 Other notable objects

5.5.1 SDSSJ113831.42+351725.3

This object contains one C IV and one Si IV BAL which show the largest absolute change in pseudo-equivalent out of any BAL of their respective ions in the entire variable BAL sample. The C IV BAL undergoes a change of $\Delta EW_p = -4142 \pm 817$, larger than the corresponding absolute change in Si IV of $\Delta EW_p = -2880 \pm 647$ km s^{-1}. However, the situation is reversed when considering the fractional change in pseudo-EW, which the Si IV BAL has a value of $\Delta EW_p/\langle EW_p \rangle = -0.979 \pm 0.245$, while for the C IV BAL

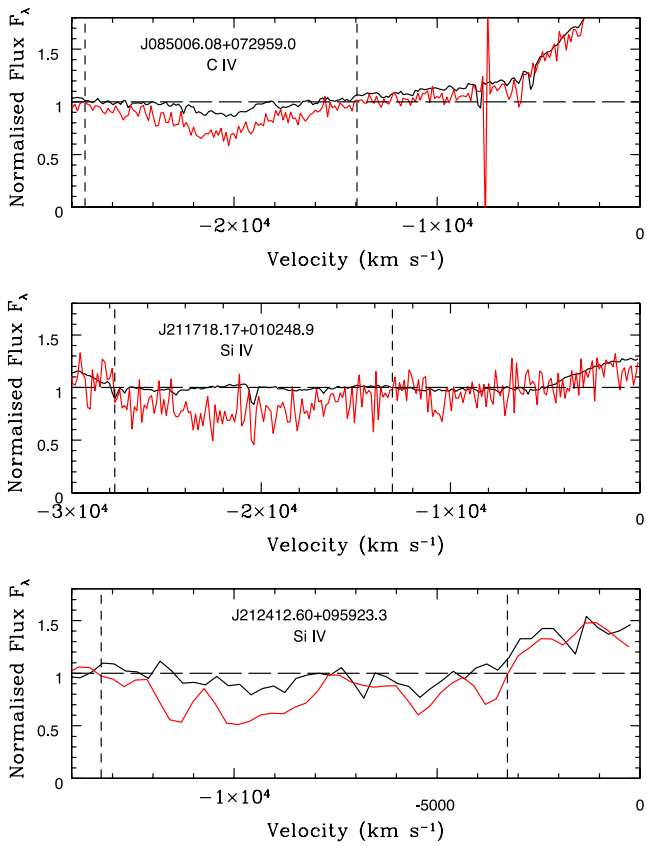

Figure 11. Disappearing BAL continuum-normalized spectra in velocity space zeroed at emission line red doublet component. Epoch 1 spectra are in red and epoch 2 in black.

it is $\Delta EW_p/\langle EW_p\rangle = -0.606 \pm 0.125$. Apart from variability, the properties of this quasar are not exceptional.

5.5.2 SDSSJ164152.30+305851.7

This is the only quasar in our sample showing evidence of LoBAL absorption, with both Mg II and Al III BALs visible in both the WHT and Gemini spectra. It is likely that a C II BAL overlaps the Si IV broad absorption in this quasar as otherwise the Si IV BAL would have extreme properties, with a pseudo-EW of $\langle EW_p\rangle = 26389 \pm 742\,km\,s^{-1}$, a width of $28661 \pm 512\,km\,s^{-1}$ and a depth of $\langle B_{depth}\rangle = 0.909 \pm 0.029$. These quantities would be by far the largest for any Si IV BAL in the variable sample (the second strongest Si IV BAL sample has $\langle EW_p\rangle = 7255 \pm 214\,km\,s^{-1}$) and would also be stronger than any C IV BAL in the variable sample, including the C IV BAL in the same object. This would be unusual as Si IV BALs are weaker than C IV BALs in every other object containing variable BALs of both kinds. Aside from the presence of LoBAL absorption, this quasar is also interesting as it exhibits a C IV BAL with the highest pseudo-EW of any C IV BAL in the variable sample ($\langle EW_p\rangle = 13526 \pm 593\,km\,s^{-1}$).

6 CONCLUSIONS

6.1 Epoch separation time and velocity dependence

By performing a comparative study using data sets from Barlow (1993), L07 and their own sample, G08 found an increase in C IV absorption variability with increased epoch separation time. We find a mean value of $|\Delta EW_p/\langle EW_p\rangle| = 0.43 \pm 0.03$ for all C IV BALs identified as variable. This compares with a mean value of $|\Delta EW_p/\langle EW_p\rangle| = 0.55 \pm 0.03$ for the sample of 16 BALs showing significant variability in L07. However, their mean is skewed by three outlying features, the lowest of which has an EW more than double that of the next most variable BAL. If these BALs are excluded, a mean value of $|\Delta EW_p/\langle EW_p\rangle| = 0.31 \pm 0.03$ is recovered, lower than the value for our sample and consistent with a positive correlation between BAL variability amplitude and epoch separation time when considering time-scales ranging from months to several years. However, the range of time-scales studied within our quasar sample is not sufficient to provide evidence of variability dependence on our epoch separation time.

We find no evidence for the proposed spike in variability in the velocity range 12000 to 15000 km s^{-1} proposed in L07. In fact, no trends are found relating the velocity width or BAL centroid velocity with variability. If variability is mainly driven by differences in covering fraction, then the absence of any correlation between BAL centroid velocity and variability amplitude could indicate that the outflow velocity along the line of sight is not well correlated with velocity across the line of sight.

6.2 What gives rise to BAL variability?

Fractional pseudo-EW variability is strongly inversely correlated with the mean BAL depth averaged over the two epochs. This is what would be expected if ionizing continuum changes altering the fractions of the ions making up the outflowing gas were responsible for variability in the strength of the BALs, as deeper troughs may indicate an optically deeper outflow. However, this is questionable for two reasons: (1) the depth measure and the epoch averaged EW show a strong positive correlation, suggesting that this relationship is an artefact of the denominator in the fractional change and (2) we find no strongly significant correlation between rest-frame *i*-band luminosity (M_i) and BAL variability. There is a moderately significant probability of an inverse correlation between absolute change in pseudo-EW and absolute *i*-band luminosity in the variable C IV BAL sample; however, under the assumption of lower luminosity sources driving stronger variability in the case where ionization

Table 7. C IV BALs showing evidence of both an absorbed continuum and unabsorbed BLR.

Object	V_{max} (km s^{-1})	V_{min} (km s^{-1})	Epoch 1 covering fraction (±10 per cent)	Epoch 2 covering fraction (±10 per cent)
SDSSJ035335.67−061802.5	−12600	−11800	0.71	0.86
SDSSJ073535.44+374450.4	−12900	−8100	0.78	0.82
SDSSJ100312.63+402505.6	−10500	−8000	0.84	0.88
SDSSJ114722.09+373720.7	−14300	−8400	0.64	0.71
SDSSJ143632.25+501403.6	−12000	−8700	0.79	0.88

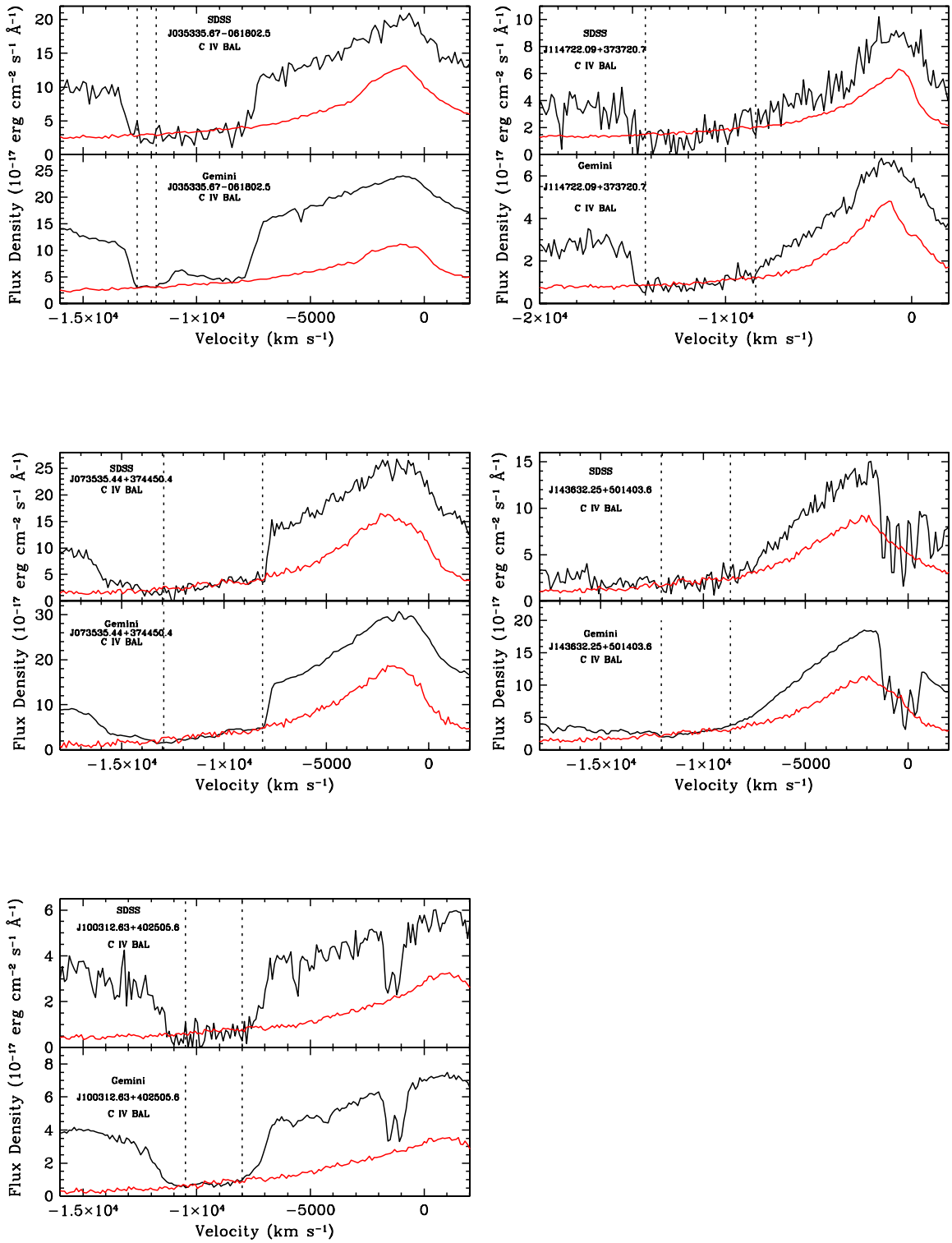

Figure 12. SDSS observations (upper panels) and Gemini/GMOS observations (lower panels) for 5 C IV BALs showing evidence for a gas geometry where the BEL is unobscured while most of the continuum region is covered by an optically thick absorber. Reconstruction minus covered continuum is in red, while observed spectrum is in black.

changes are responsible, it would be expected that we would see a corresponding signal indicating absolute change in pseudo-EW is inversely correlated with $\langle B_{\rm depth} \rangle$ for C IV BALs, which is not found. In fact, Si IV BALs show a moderate probability of the same correlation, leading to the conclusion that there are no real correlations in these cases and that there is no strong evidence for ionization changes driving BAL variability.

An alternative explanation is that the observed variability is driven by covering fraction changes. One such possibility is an inhomogeneous absorber model in which the column density along the

line of sight is due to clumpy absorbers which can move laterally into and out of the line of sight at any radial distance from the continuum source. The clumpy inhomogeneous model has received support from Capellupo et al. (2012) who found the strongest variability within small velocity regions of BAL troughs, which may correspond to movements of individual clouds with narrow velocity ranges. An alternative to the inhomogeneous absorber model is a so-called pure partial coverage scenario in which the gas is relatively homogeneous along the radial axis but moves laterally with respect to the line between the Earth and the quasar emission region.

The Si IV BALs are observed to vary more often than the C IV BALs and within those quasars that show both types of BAL varying, the Si IV BALs undergo the greatest fractional variability. This evidence would seem to favour the clumpy model over the homogeneous scenario as it could be due to an outflow in which the greater column density of C IV ions over Si IV means that C IV is more likely to be saturated. In such an outflow, a cloud moving into the line of sight may not affect the absorption line profile since a particular cloud would be entering into a portion of the outflowing column which is already opaque at the narrow range of wavelengths that the cloud could absorb. This could result in a scenario where a column of clumpy absorbers only partially covers the emission from the quasar, but due to the spatial extent along the line of sight of the entire outflow, a cloud moving into the line of sight does not affect the absorption profile. Higher frequency of saturation of C IV as compared to Si IV (due to the greater abundance of carbon compared to silicon, or possibly ionization effects favouring C IV over Si IV) is also supported by the fact that of the five quasars showing BALs with an uncovered BLR and covered continuum, the uncovered BLR emission spectra do not fit the Si IV BAL profiles. In such a saturated C IV BAL case, moving clouds into and out of the line of sight would not significantly change the depth of C IV troughs when compared with Si IV variability.

The fact that the 14 quasars showing variability in both ions have BALs with largely overlapping outflow velocities, in which the direction of change is the same, strong evidence for the two types of BAL being part of the same outflow and influenced by the same variability mechanism in these cases. The sample of nine quasars showing one type of BAL varying while the other does not, with substantial velocity overlap between the two, seems to contradict such a conclusion. However, the variable BAL in seven of these cases is Si IV, while the C IV BAL does not vary. If C IV is saturated in these cases, this would allow Si IV to vary without affecting the C IV BAL variability amplitude in the overlapping velocity range, allowing consistency with the clumpy absorber model.

Despite this, ionization changes are not entirely ruled out as a driver of BAL variability. The luminosity dependence that was used as a proxy for extreme-ultraviolet (EUV) variability is two steps removed from a direct observation of the ionizing continuum flux and it is possible that the complexity of the response of the outflowing gas to ionizing continuum changes may not be analogous to that of the emission lines. The hint of a positive correlation between the fractional variability of Si IV and C IV where an approximately linear relationship exists between the two quantities with a gradient not equal to 1 (see Section 5.1) would seem to fit more naturally with ionizing continuum variability as the explanation rather than gas line of sight changes. However, this is far from certain given the value of only 98 per cent correlation probability derived from Spearman rank test and the fact that the least-squares fit line only appears to fit 8 out of the 14 quasars showing variability in both types of BAL. Other possible indicators of ionizing continuum changes include 2 cases of C IV variability which are *unaccompanied* by Si IV variability at the same velocities. This is hard to explain in terms of gas covering fraction changes as it would require some sort of spatial separation between Si IV and C IV outflows. Calculations of theoretical ionization fractions across ionization parameter space suggest that this is unlikely as there is substantial overlap in the log ion fraction versus log ionization parameter curves of each ion (see fig. 4 in Hamann et al. 2001).

Future investigations may be able to find more definitive evidence for continuum variations by accurately measuring continua in a high S/N quasar sample across several epochs with photometric quality spectra and looking for correlations with BAL variability. An underlying assumption in investigations into continuum variability correlations with BAL variability is that the outflowing gas is dense enough to undergo recombinations on relatively short time-scales. Although the column densities of absorbers can be estimated using optical depth calculations (these are lower limits in the case of non-black saturation), the extent of the BAL flow is still a subject of debate, with estimates placing the flow as far as the kiloparsec scale from the central engine (Dunn et al. 2010). If this was the case, given the estimated outflow column densities of $\log N_{\rm H} \approx 21$ to 22 cm^{-2} (Hamann et al. 2008) the gas density could be as low as ≈ 10 cm^{-3}. Given a recombination coefficient value of $\approx 10^{-11}$ cm^3 s^{-1} for C IV and Si IV and assuming that the gas is almost completely ionized, recombination time-scales could be as long as a few hundred years. Attempts to find correlations between luminosity or continuum variability and BAL variability would in this case give no insight into how ionizing continuum changes affect the outflowing gas.

In order to gain a greater insight into the physical influences driving BAL variability, larger BALQSO sample sizes are needed. The ongoing Baryon Oscillation Spectroscopic Survey (BOSS), part of the SDSS-III (Eisenstein et al. 2011) should prove helpful in this regard. One of the ancillary projects conducted as part of this survey will provide much greater numbers of BALQSO repeat observations on multiyear time-scales than previous studies by comparing BOSS BALQSO spectra with earlier SDSS-I and II data (Filiz Ak et al. 2012).

6.3 BAL disappearance and BAL lifetimes

The fraction of C IV BALs in our sample which disappear is 1.7 per cent, lower than the 5.3 per cent value found for Si IV BALs. However, this results from only three examples of BAL disappearance, so definitive conclusions are not drawn, except to say that the disappearance rate for C IV is broadly consistent with that found in Filiz Ak et al. (2012). If Si IV BALs do show a greater tendency to disappear, this would fit in with the general picture of Si IV BALs exhibiting greater occurrences of variability and greater amplitudes of variability in a variable BAL sample. The disappearing BALs are weaker than average, as are the BALs which appear. In fact the disappearing C IV BAL is the weakest of all the C IV BALs in the variable sample. This conforms with the tendency of shallower BALs to exhibit stronger fractional variability.

The average lifetime of a BAL can be estimated by dividing the fraction of BALs that disappear by the average rest-frame lifetime of the observations. This gives an average BAL rest-frame lifetime of ≈ 142 years for C IV and ≈ 43 years for Si IV based on the time-scales and disappearing fractions from our sample. Our estimated C IV lifetime is similar to the value of 109^{+31}_{-22} years estimated in Filiz Ak et al. (2012).

6.4 Outflow geometry insight provided by covered-continuum-uncovered-BLR subsample

Reverberation studies of the variable continuum and BEL region in AGN, indicate that the 'size' of the BLR scales with ultraviolet (UV) ionizing continuum luminosity such that $R \propto L_{\rm UV}^{1/2}$ (Bentz et al. 2006), as predicted by photoionization models. The luminosities of the five objects showing evidence of C IV BALs shaped by a covered continuum+uncovered BLR are not biased towards more or less luminous objects. This indicates that the difference between this sample and other BAL quasars is not due to a smaller BLR and is instead determined by the geometry of the outflow along the line of sight. Given that the shape of the troughs in this subsample is well modelled by a mostly absorbed continuum and an entirely unobscured BLR, the maximum characteristic radius of any clumpy absorber clouds would have to be similar to the UV continuum emitting region size. Assuming that the central supermassive black hole is accreting at close to the Eddington rate and a peak ionizing UV continuum temperature corresponding to a photon energy of ≈50 eV, the ratio of the UV luminosity to the bolometric luminosity will be of the order of $\approx 10^{-1}$ (Kelly et al. 2008). Given the bolometric luminosity span of these five objects (obtained from Shen et al. 2011) the size of the UV continuum emitting region and hence the maximum size of an obscuring cloud will be in the range $\approx 10^{13}$ to 10^{14} cm. Two possibilities therefore exist, either the characteristic size of the clouds or the radius (across the line of sight) of a homogeneous outflow column must be able to vary greatly between objects, from continuum region size up to $\approx R_{\rm BLR}$, or the radius of the absorbing column emerging from the disc can vary between quasars by having considerably different numbers of approximately UV continuum emitting region sized clouds across the sight line.

7 SUMMARY

A brief summary of the main results is provided here.

(1) Si IV BALs are more likely to be variable than C IV BALs (58 versus 46 per cent, respectively). Within the sample of variable BALs, the average fractional change in pseudo-EW is higher for Si IV BALs (0.577 versus 0.367 for C IV BALs when excluding the LoBAL quasar SDSSJ164152.30+305851.7).

(2) Both Si IV and C IV BALs have fractional changes in pseudo-EW which are strongly correlated (greater than 99.9 per cent significance) with their epoch averaged depths. We suggest that this is a result of the strong positive correlation between BAL depth and pseudo-EW rather than a real physical effect. No strong evidence is found of absolute change in pseudo-EW dependence on epoch averaged pseudo-EW, nor any correlation of absolute change in pseudo-EW with BAL depth or width.

(3) No correlation is found between BAL variability and the absolute *i*-band luminosity of their host quasars. Since ionizing continuum changes drive BEL variability, this result suggests that variability of the ionizing continuum does not play a significant role in BAL variability, assuming that the outflowing gas is in ionization equilibrium with the photoionizing continuum.

(4) Within each of the 14 quasars exhibiting both a varying Si IV and a varying C IV BAL, the change in pseudo-EW is in the same direction (strengthening or weakening) across the two BALs. Furthermore, each of these objects show significant overlap in velocity space of the spectral regions spanning the two, suggesting that the BALs of both ions originate in the same outflow. There is marginal evidence (98 per cent significance) that the fractional change in pseudo-EW of Si IV and C IV BALs is correlated.

(5) Examples of both BAL appearance and disappearance are found, with instances in both Si IV (3 appearance, 2 disappearance) and C IV (1 appearance, 1 disappearance). Their relative recurrence rates suggest Si IV and C IV BAL lifetimes of 43 years and 142 years, respectively. Appearing and disappearing BALs are weaker than average, complying with the general trend noted in point 2.

(6) There is evidence in five objects of a mostly covered continuum region combined with an uncovered BLR. This can be seen as a trough profile in deep C IV BALs which follows the emission line profile once a substantial fraction of the continuum has been subtracted. This suggests a range in maximum cloud radius for the clumpy inhomogeneous absorber model of $\approx 10^{13}$ to 10^{14} cm for the outflows from these quasars, assuming that accretion is close to the Eddington rate.

ACKNOWLEDGEMENTS

This work is supported at the University of Leicester by the Science and Technology Facilities Council (STFC) and is partly based on observations obtained at the Gemini Observatory, which is operated by the Association Research in Astronomy, Inc., under a cooperative agreement with the NSF on behalf of the Gemini partnership. It is also based on observations made with the WHT/ISIS operated on the island of La Palma by the Isaac Newton Group in the Spanish Observatorio del Roque de los Muchachos of the Instituto de AstrofÃsica de Canarias and spectroscopic observations from Data release 6 of the SDSS. We wish to thank our anonymous referee for their useful comments and thorough review of the draft. JTA acknowledges the award of an ARC Super Science Fellowship.

Funding for the SDSS and SDSS-II has been provided by the Alfred P. Sloan Foundation, the Participating Institutions, the National Science Foundation, the US Department of Energy, the National Aeronautics and Space Administration, the Japanese Monbukagakusho, the Max Planck Society and the Higher Education Funding Council for England. The SDSS website is http://www.sdss.org/.

The SDSS is managed by the Astrophysical Research Consortium for the Participating Institutions. The Participating Institutions are the American Museum of Natural History, Astrophysical Institute Potsdam, University of Basel, University of Cambridge, Case Western Reserve University, University of Chicago, Drexel University, Fermilab, the Institute for Advanced Study, the Japan Participation Group, Johns Hopkins University, the Joint Institute for Nuclear Astrophysics, the Kavli Institute for Particle Astrophysics and Cosmology, the Korean Scientist Group, the Chinese Academy of Sciences (LAMOST), Los Alamos National Laboratory, the Max-Planck-Institute for Astronomy (MPIA), the Max-Planck-Institute for Astrophysics (MPA), New Mexico State University, Ohio State University, University of Pittsburgh, University of Portsmouth, Princeton University, the United States Naval Observatory and the University of Washington.

REFERENCES

Adelman-McCarthy J. K., Agüeros M. A., Allam S. S., Anderson K. S., 2007, ApJS, 172, 634

Allen J. T., Hewett P. C., Maddox N., Richards G. T., Belokurov V., 2011, MNRAS, 410, 860

Arav N., Becker R. H., Laurent-Muehleisen S. A., Gregg M. D., White R. L., Brotherton M. S., de Kool M., 1999, ApJ, 524, 566

Barlow T. A., 1993, PhD thesis, California University

Barlow T. A., 1994, PASP, 106, 548
Bentz M. C., Peterson B. M., Pogge R. W., Vestergaard M., Onken C. A., 2006, ApJ, 644, 133
Blandford R. D., McKee C. F., 1982, ApJ, 255, 419
Bottorff M., Korista K. T., Shlosman I., Blandford R. D., 1997, ApJ, 479, 200
Capellupo D. M., Hamann F., Shields J. C., Rodríguez Hidalgo P., Barlow T. A., 2011, MNRAS, 413, 908
Capellupo D. M., Hamann F., Shields J. C., Rodríguez Hidalgo P., Barlow T. A., 2012, MNRAS, 422, 3249
Capellupo D. M., Hamann F., Shields J. C., Halpern J. P., Barlow T. A., 2013, MNRAS, 429, 1872
Cardelli J. A., Clayton G. C., Mathis J. S., 1989, ApJ, 345, 245
Chelouche D., Netzer H., 2001, MNRAS, 326, 916
Cottis C. E., Goad M. R., Knigge C., Scaringi S., 2010, MNRAS, 406, 2094
Dunn J. P. et al., 2010, ApJ, 709, 611
Eisenstein D. J. et al., 2011, AJ, 142, 72
Elvis M., 2000, ApJ, 545, 63
Everett J. E., 2005, ApJ, 631, 689
Filiz Ak N., Brandt W. N., Hall P. B., Schneider D. P., 2012, ApJ, 757, 114
Gibson R. R., Brandt W. N., Schneider D. P., Gallagher S. C., 2008, ApJ, 675, 985 (G08)
Gibson R. R., Brandt W. N., Gallagher S. C., Hewett P. C., Schneider D. P., 2010, ApJ, 713, 220 (G10)
Giustini M., Proga D., 2012, ApJ, 758, 70
Gunn J. E., Carr M., Rockosi C., Sekiguchi M., Berry K., Elms B., de Haas E., 1998, AJ, 116, 3040
Hall P. B., Anderson S. F., Strauss M. A., York D. G., Richards G. T., Fan X., Knapp G. R., 2002, ApJS, 141, 267
Hamann F. W., Barlow T. A., Chaffee F. C., Foltz C. B., Weymann R. J., 2001, ApJ, 550, 142
Hamann F., Kaplan K. F., Rodríguez Hidalgo P., Prochaska J. X., Herbert-Fort S., 2008, MNRAS, 391, L39
Hamann F., Kanekar N., Prochaska J. X., Murphy M. T., Ellison S., Malec A. L., Milutinovic N., Ubachs W., 2011, MNRAS, 410, 1957
Hamann F., Chartas G., McGraw S., Rodriguez Hidalgo P., Shields J., Capellupo D., Charlton J., Eracleous M., 2013, MNRAS, 435, 133
Hewett P. C., Wild V., 2010, VizieR Online Data Catalog, 740, 52302
Kelly B. C., Bechtold J., Trump J. R., Vestergaard M., Siemiginowska A., 2008, ApJS, 176, 355
King A. R., 2010, MNRAS, 402, 1516
Knigge C., Scaringi S., Goad M. R., Cottis C. E., 2008, MNRAS, 386, 1426
Lundgren B. F., Wilhite B. C., Brunner R. J., Hall P. B., Schneider D. P., York D. G., Vanden Berk D. E., Brinkmann J., 2007, ApJ, 656, 73 (L07)
Lupton R., Gunn J. E., Ivezić Z., Knapp G. R., Kent S., Yasuda N., 2001, in Harnden F. R., Jr, Primini F. A., Payne H. E., eds, ASP Conf. Ser. Vol. 238, The SDSS Imaging Pipelines. Astron. Soc. Pac., San Francisco, p. 269
Magorrian J. et al., 1998, AJ, 115, 2285
Narayanan D., Hamann F., Barlow T., Burbidge E. M., Cohen R. D., Junkkarinen V., Lyons R., 2004, ApJ, 601, 715
Peterson B. M., Wanders I., Bertram R., Hunley J. F., Pogge R. W., Wagner R. M., 1998, ApJ, 501, 82
Proga D., Stone J. M., Kallman T. R., 2000, ApJ, 543, 686
Reichard T. A. et al., 2003a, AJ, 125, 1711
Reichard T. A. et al., 2003b, AJ, 126, 2594
Rodriguez Hidalgo P. R., Hamann F., Eracleous M., Capellupo D., Charlton J., Shields J., 2012, in Chartas G., Hamann F., Leighly K. M., eds, ASP Conf. Ser. Vol. 460, Variability of Mini-BAL and BAL Outflows in Quasars. Astron. Soc. Pac., San Francisco, p. 93
Scaringi S., Cottis C. E., Knigge C., Goad M. R., 2009, MNRAS, 399, 2231
Schlegel D. J., Finkbeiner D. P., Davis M., 1998, ApJ, 500, 525
Schmidt G. D., Hines D. C., 1999, ApJ, 512, 125
Schneider D. P., Richards G. T., Hall P. B., Strauss M. A., Anderson S. F., Boroson T. A., 2010, AJ, 139, 2360
Shen Y. et al., 2011, ApJS, 194, 45
Silk J., Rees M. J., 1998, A&A, 331, L1
Sprayberry D., Foltz C. B., 1992, ApJ, 390, 39
Springel V., Di Matteo T., Hernquist L., 2005, MNRAS, 361, 776
Stoughton C., Lupton R. H., Bernardi M., Blanton M. R., Burles S., Castander F. J., Connolly A. J., 2002, AJ, 123, 485
Trump J. R. et al., 2006, ApJS, 165, 1
Turnshek D. A., 1988, in Blades J. C., Turnshek D. A., Norman C. A., eds, QSO Absorption Lines: Probing the Universe. Cambridge Univ. Press, Cambridge, p. 17
Vanden Berk D. E., Wilhite B. C., Kron R. G., 2004, ApJ, 601, 692
Vivek M., Srianand R., Mahabal A., Kuriakose V. C., 2012, MNRAS, 421, L107
Weymann R. J., Morris S. L., Foltz C. B., Hewett P. C., 1991, ApJ, 373, 23
Wilhite B. C., Vanden Berk D. E., Brunner R. J., Brinkmann J. V., 2006, ApJ, 641, 78
York D. G., 2000, AJ, 120, 1579

This paper has been typeset from a TEX/LATEX file prepared by the author.